The Thesis Committee for Jarrod Robert Zaborac
Certifies that this is the approved version of the following thesis:

Crack-Based Damage Assessment of In-Service Reinforced Concrete Bridge Members

APPROVED BY
SUPERVISING COMMITTEE:

Supervisor:

Trevor Hrynyk

Oguzhan Bayrak

Crack-Based Damage Assessment of In-Service Reinforced Concrete Bridge Members

by

Jarrod Robert Zaborac

Thesis

Presented to the Faculty of the Graduate School of

The University of Texas at Austin

in Partial Fulfillment

of the Requirements

for the Degree of

Master of Science in Engineering

The University of Texas at Austin

August 2017

Dedication

To my family and friends, both near and far

Acknowledgements

My sincerest thanks to both TxDOT and the Center for Transportation Workforce Development of the FHWA for providing the funding which made both this project and my involvement in it possible. Both organizations have afforded me wonderful opportunities to expand my education, for which I am grateful.

Dr. Hrynyk's patience and advice throughout my master's work has been much appreciated and has helped me grow as a structural engineer. Additionally, thanks to Dr. Hrynyk and Dr. Bayrak for their assistance in reading and editing my thesis.

I would also like to my family for helping to get me where I am in life and always supporting me while I pursue my dreams, even when it meant I had to move a very long drive away. Thank you.

Abstract

Crack-Based Damage Assessment of In-Service Reinforced Concrete Bridge Members

Jarrod Robert Zaborac, M.S.E.

The University of Texas at Austin, 2017

Supervisor: Trevor Hrynyk

Reinforced concrete bridge infrastructure is typically evaluated based on visually observed cracking/damage. However, traditional inspection procedures typically provide little-to-no insight into the remaining capacity of the inspected member. Although more rigorous methods have been proposed in the literature that offer quantitative insight into a structure's health (with various levels of success), no procedure has been widely adopted. Furthermore, many of these proposed procedures have not been validated by experimental data.

Experimental visual crack data were collected into a database to provide researchers and practitioners a means of developing and evaluating crack-based shear strength assessment procedures. The database has an emphasis on members which are similar in detail or scale to typical bridge elements. The database was subsequently used to evaluate a proposed mechanics-based damage assessment procedure based on an inverse solution of the modified compression field theory. In addition to visually observed crack characteristics (e.g., crack width and inclination), the proposed procedure relies upon basic

material properties and design details. Average load proportions are estimated as a part of the procedure, therefore actual loading conditions (e.g., $M/V \cdot d$ ratio for a beam) need not be known to calculate an estimate of an element's residual capacity.

Results from 420 analyses on beams from three experimental programs carried-out with the procedure show the potential of a mechanics-based procedure for the crack-based shear strength assessment of reinforced concrete bridge members. The average predicted-to-experimental ratio for normalized shear strength (i.e., capacity-in-use) was reasonable for two of the experimental series (0.98 – 1.17); however, results from the third group of beams trended much more conservatively (average predicted-to-experiment ratio of 1.43). Overall, the procedure is relatively simple and general in its application and shows promise as an evaluation tool.

Table of Contents

List of Tables

List of Figures

Chapter 1: Introduction

1.1 OVERVIEW

Approximately 9.1 % of bridges in the United States are considered "structurally deficient" according to the 2017 Infrastructure Report Card. Furthermore, nearly 40 % of the nation's 614,000 bridges are now more than 50 years old (ASCE, 2017). Thus, there is a need for reliable bridge inspection and assessment procedures, and it is expected that this need will increase in the years to come.

Traditional reinforced concrete (RC) bridge inspection procedures have typically relied on visual-observations of the in-service conditions of a bridge member or element; however, these kinds of procedures are generally more qualitative in nature and provide little-to-no insight regarding the actual structural (i.e., load resisting) adequacies of in-service structures. Many supplementary bridge inspection procedures have been proposed in the literature to address this deficiency (e.g., empirical methods, finite element analysis, etc.), but there has been little consensus on the determination of a method that is both general enough for application to the broad range of RC bridge members encountered in practice and simple to use. One potential solution is the application of a mechanics-based RC assessment procedure that incorporates the effects of member detailing, scale, and loading conditions. Very few such procedures have been proposed in the literature and even fewer have been experimentally validated. To this end, a preliminary analytical study focused on the development of simple-to-use mechanics-based RC assessment tools was carried-out. Further, the application of these tools is aimed at performing crack-based quantitative assessments of RC bridge elements that are encountered in the State of Texas.

A secondary, but directly-related, objective of this thesis was to develop a visual crack measurement database as a means of:

- Developing new crack-based shear strength assessment procedures
- Evaluating new and existing crack-based shear strength assessment procedures
- Providing visual benchmarks for field data
- Serving as a resource for future projects focused on related research areas

A preliminary mechanics-based procedure method was proposed to assess damaged RC elements based on visually observed concrete cracking. The mechanics-based procedure uses the formulations of the Modified Compression Field Theory (MCFT) (Vecchio and Collins, 1986) at its core, and employs supplementary models (CEB-FIP, 1978; Uzel, 2003) to provide residual capacity estimates for cracked RC elements. Preliminary procedure appraisal was completed using data reported from three experimental series (Birrcher et al., 2009; Bracci et al., 2000; Larson et al., 2013). The procedure showed promise as a means of estimating residual capacity and giving insight into future structural behavior.

The results presented in this thesis show general trends in a large volume of crack data and proof-of-concept for a relatively simple crack-based shear strength assessment procedure. As the assessment of infrastructure nearing the end of its service life becomes more necessary, these tools can provide a springboard for effective and practical means of evaluating the adequacies of deteriorating RC structures and/or the need for remedial actions.

1.2 TEXAS FIELD DATA REVIEW

To identify relevant member types experiencing RC crack-related problems in Texas, available field data from in-service Texas Department of Transportation (TxDOT)

bridges were collected and reviewed. A previous project completed at The University of Texas at Austin, TxDOT Project 0-6416, had compiled relevant structural cracking measurements, member details, and associated photographs from across the state of Texas. Additionally, consultation with TxDOT personnel identified additional sites and the common problems associated with aging infrastructure in Texas.

TxDOT project report 0-6416-1 (Larson et al., 2013) contains a summary of eight in-service inverted-T bridge bents with noteworthy diagonal cracking. Locations include the following cities: Austin, El Paso, San Antonio, and Waco. A sample photograph and the crack pattern documentation provided in the report is shown in Figure 1-1. Additional information, including plans, details, and photographs, was also compiled into an Excel database by TxDOT personnel.

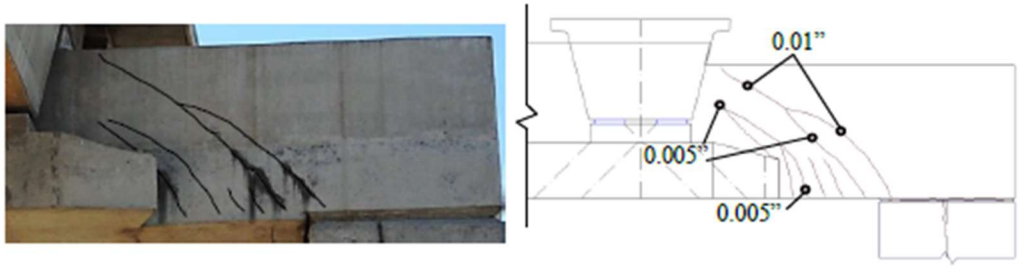

Figure 1-1: Crack size and location on the northwest corner of Waco bent 17 (Larson et al., 2013)

Subsequent correspondence with TxDOT personnel also yielded the following bridges with cracking-related concerns: Interstate Highway 20 Eastbound and Westbound at State Highway 351 and FM 652 at Salt Creek. Issues at these sites included cracked straddle caps and pan girders. Furthermore, diagonal cracking in cantilever bent caps has been identified as an area of concern across the state. Figure 1-2 shows locations where cracking has been recorded as potential areas of concern for the bridge's maintenance cycle.

Figure 1-2: Locations where cracking is a potential concern

1.3 RESEARCH OBJECTIVES

As infrastructure deteriorates and the need to reliably examine damaged RC structures increases, the methods that engineers and inspectors use to monitor and assess in-service structures must also mature. Thus, the primary goals of this thesis are as follows:

1. Develop a visual crack measurement database to assist in developing new crack-based shear strength assessment procedures, evaluating new and existing crack-based shear strength assessment procedures, providing visual benchmarks for field data, and serving as a resource for future projects focused on related research areas.

2. Develop a preliminary procedure for crack-based RC shear strength assessment using concrete mechanics formulations.
3. Evaluate the preliminary procedure using the database for the purposes of determining the adequacy of the assessment procedure and the usefulness of the database as an evaluation tool for crack-based shear strength member assessment.

1.4 ORGANIZATION

This thesis contains five chapters. After this introductory chapter is Chapter 2, which provides a brief overview of many of the currently available methods that have been used for assessing cracked RC elements. Chapter 3 discusses the creation of a Visual Crack Measurement Database and its potential applications. Chapter 4 proposes and appraises a preliminary mechanics-based procedure for the crack-based assessment of RC bridge elements. Lastly, Chapter 5 discusses conclusions made from the work presented in Chapters 3 and 4 and provides recommendations for future work.

Chapter 2: Literature Review

This chapter reviews methods for the assessment of damaged, in-service RC elements. The chapter is divided into two main sections: visual inspection methods and residual capacity estimate methods. There are several methods available for each category; however, the visual inspection methods are more commonly used in practice while the residual capacity estimates are yet to be widely established and/or adopted. Each method has its own strengths and weaknesses, which are briefly discussed in this chapter.

2.1 TOOLS EMPLOYED IN PRACTICE

Current methods used for the evaluation of RC structures rely on several different standards. For bridges and other transportation-related infrastructure, Department of Transportation (DOT) requirements vary slightly from state to state, but can ultimately be tied back to guidelines from two organizations: the Federal Highway Administration (FHWA) and the American Association of State Highway and Transportation Officials (AASHTO). Falling outside of transportation infrastructure, the International Atomic Energy Agency (IAEA) is another source that provides tools for the assessment of damaged RC structures and details on inspection methods ranging from visual to more advanced techniques.

The FHWA maintains a database of the nation's bridges called the National Bridge Index (NBI). The *Recording and Coding Guide of the Structure Inventory and Appraisal of the Nation's Bridges* (FHWA, 1995) provides a standard for recording relevant data to meet federal requirements. A majority of the information stored on the "Structure Inventory and Appraisal Sheet" is related to identifying and locating the bridge as well as classifying geometric and navigation data. Of interest for the damage assessment of in-service bridges is the "Condition" subsection, which contains lines for coding the condition of the deck,

superstructure, and substructure. Channel and channel protection, as well as culverts, also have condition ratings. The condition ratings are done using the ten-point scale shown in Table 2-1.

Table 2-1: FHWA codes and descriptions (reproduced from FHWA, 1995)

Code	Description
N	NOT APPLICABLE
9	EXCELLENT CONDITION
8	VERY GOOD CONDITION – no problems noted.
7	GOOD CONDITION – some minor problems.
6	SATISFACTORY CONDITION – structural elements show some minor deterioration.
5	FAIR CONDITION – all primary structural elements are sound but may have minor section loss, cracking, spalling or scour.
4	POOR CONDITION – advanced section loss, deterioration, spalling or scour
3	SERIOUS CONDITION – loss of section, deterioration, spalling or scour have seriously affected primary structural components.
2	CRITICAL CONDITION – advanced deterioration of primary structural elements. Fatigue cracks in steel or shear cracks in concrete may be present or scour may have removed substructure support. Unless closely monitored it may be necessary to close the bridge until corrective action is taken.
1	"IMMINENT" FAILURE CONDITION – major deterioration or section loss present in critical structural components or obvious vertical or horizontal movement affecting structure stability. Bridge is closed to traffic but corrective action may put back in light service.
0	FAILED CONDITION – out of service – beyond corrective action.

Additionally, the "Load Rating and Posting" subsection of the guidelines classify the operating rating and the maximum load considered safe for the structure. The following methods are permissible for calculating this value: load factor (LF), allowable stress (AS), load and resistance factor (LRFR), and load testing. These methods use the ratings from Table 2-1, among other design details, to apply a reduction to the capacity. The condition factor from the LRFR method is divided into three categories: good or satisfactory (1.00), fair (0.95), or poor (0.85). These factors are analogous to typical safety factors from the traditional design process, that is, the factors are associated with anticipated variability in capacity based on member deterioration (AASHTO, 2005). The LF method is used for

recording in the NBI, although the other methods may be used for posting. Additional information and tools are available in the appendices, such as the Sufficiency Rating Formula, which can be used to estimate a bridge's serviceability. Note that this is not necessarily indicative of structural capacity; however, a bridge inspector may use this rating to assist in making decisions about whether a bridge should remain in service.

AASHTO produces the *AASHTO Bridge Element Inspection Manual* (2010) which, when used as input in the bridge management system provided by the FHWA, is considered a satisfactory substitute for these provisions. While the *Recording and Coding Guide of the Structure Inventory and Appraisal of the Nation's Bridges* uses a broad rating system for deck, superstructure, and substructure, the *Bridge Element Inspection Manual* (AASHTO, 2010) contains more explicit guidance for the classification of various bridge elements. Additionally, the rating system uses four condition states, rather than the ten-point code system. Table 2-2 shows condition states and descriptions of typical defects associated with a RC closed web/box girder element. Table 2-3 provides some quantitative guidance on the qualitative traits (e.g., hairline, narrow, and medium) given in Table 2-2, to assist condition state classification. The IAEA (2002) *Guidebook on Nondestructive Testing of Concrete Structures*, while not typically adopted by DOTs, uses a very similar rating system as the *Bridge Element Inspection Manual* (2010); furthermore, the guidebook provides additional details pertaining to more in-depth nondestructive testing procedures such as ultrasound or infrared thermography.

Table 2-2: Condition state definitions for RC closed web/box girder elements (reproduced from AASHTO, 2010)

Defect	Condition State 1	Condition State 2	Condition State 3	Condition State 4
Cracking	None to hairline	Narrow size and/or density	Medium size and/or density	The condition is beyond the limits in condition state (3) and/or warrants a structural review to determine the strength or serviceability of the element or bridge.
Spalls/ Delaminations/ Patched Areas	None	Moderate spall or patch areas that are sound	Severe spall or patched area showing distress	
Efflorescence	None	Moderate without rust	Severe with rust staining	
Load Capacity	No reduction	No reduction	No reduction	

Table 2-3: Defect Guidelines (reproduced from AASHTO, 2010)

Defect	Hairline-Minor	Narrow- Moderate	Medium-Severe
Cracking	< 0.0625 inches (1.6 mm)	0.0625 – 0.125 inches (1.6 – 3.2 mm)	> 0.125 inches (3.2 mm)
Spalls/ Delaminations	N/A	Spall less than 1 inch (25 mm) deep or less than 6 inches in diameter	Spall greater than 1 inch (25 mm) deep or greater than 6 inches in diameter or exposed rebar
Cracking Density	Spacing Greater than 3.0 feet (0.33 m)	Spacing of 1.0 – 3.0 feet (0.33 – 1.0 m)	Spacing of less than 1 foot (0.33 m)
Efflorescence	N/A	Surface white without build-up or leaching	Heavy build-up with rust staining

Many states have published their own reference manuals or tools that provide more state specific guidance for bridge inspection (MDOT, 2011; MDT, 2015; ODOT, 2014; ODOT, 2009; PennDOT, 2009; TxDOT, 2013). These publications vary from state to state and range from summaries and modifications of federal standards to "pocket coding guides" to create a standardized, uniform inspection process across the state. For example, the ODOT (2009) *Bridge Inspection Pocket Coding Guide* uses the provisions from the *AASHTO Bridge Element Inspection Manual*, but includes visual standards, shown in Figure 2-1, to assist in the classification of the condition state of a structural element.

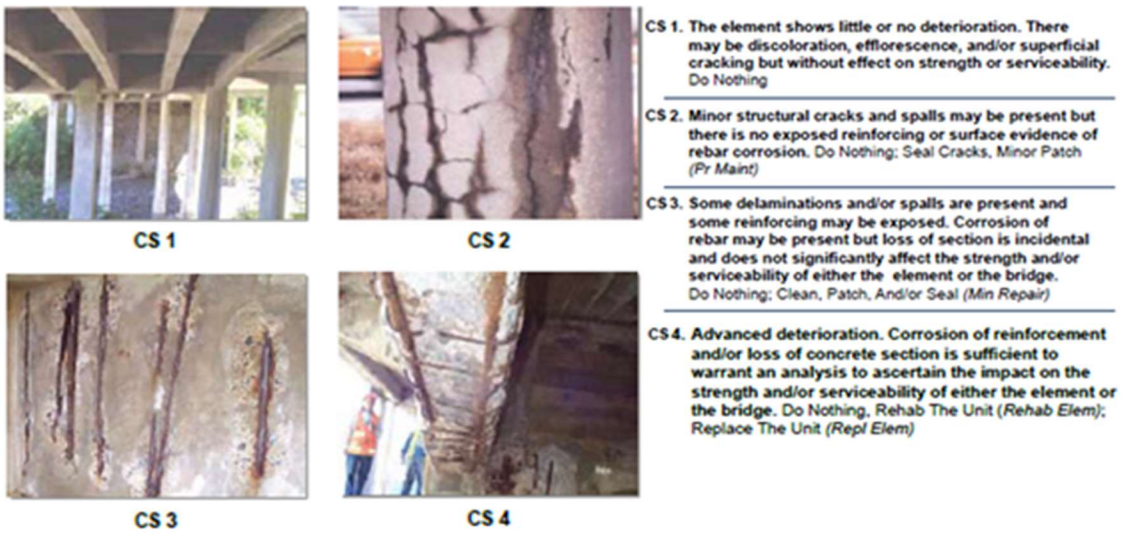

Figure 2-1: Visual reference for evaluating condition states (ODOT, 2009)

2.2 Structural Assessment of RC Infrastructure Based on Observed Damage

In addition to the visual inspection tools discussed in the previous section, there are several, generally more rigorous assessment methods proposed in the literature. These methods provide quantitative assessments, while those detailed in the Section 2.1 are much more qualitative in nature. These quantitative assessment methods attempt to estimate the residual capacity of a RC element using a variety of techniques, such as empirical models (e.g., curve-fitting, statistical tools, etc.) or theoretical models (e.g., finite element analysis, mechanics, etc.).

To address the quantitative shortcomings of the tools presented in Section 2.1, several researchers (Abi Shdid et al., 2006; Gulkan & Yakut, 1996; Melchor-Lucero & Ferregut, 1996; Paal et al., 2015; Veletzos et al., 2008) have attempted to correlate visually observed damage to residual capacity estimations. Typically, these methods rely on a visual rating or qualifier to characterize the level of damage to provide the estimation. One

example (Abi Shdid et al., 2006) used a four-point rating scale as a means of estimating capacity loss; however, the results provided limited successes. Several of the methods (Gulkan & Yakut, 1996; Melchor-Lucero & Ferregut, 1996; Paal et al., 2015; Veletzos et al., 2008) were specifically for seismic-related damage; as such, they may not be generally applicable to all cases observed in practice.

Another approach to correlating visually observed damage to residual capacity in cracked RC bridge elements is to create a family of solutions based on experimental results (Birrcher et al., 2009; Larson et al., 2013) which capture the influence of relevant variables such as web reinforcement ratios, shear span-to-depth ratios, effective depth, etc. These solutions may be documented in charts or graphically, as shown in Figure 2-2 and Figure 2-3. Using very little input and computational power, load levels (and thereby residual capacity) can be estimated with a reasonable level of confidence (typically 10 to 15 %). However, the scope of these methods in practice is limited to the scope of the experimental data they were calibrated with and may lack the generality necessary to assess all cases encountered in practice.

Load on the Member, Quantified as a Percent of Ultimate Capacity on Average (± scatter)						
Reinforcement \ w_{max} (in.)	0.01	0.02	0.03	0.04	0.05	0.06
$\rho_v = 0.002$ $\rho_h = 0.002$	20 (+10)	30 (±10)	40 (±10)	50 (±10)	60 (±15)	70 (±15)
$\rho_v = 0.003$ $\rho_h = 0.003$	25 (±10)	40 (±10)	55 (±10)	70 (±10)	80 (±10)	90 (±10)
$\rho_v > 0.003$ $\rho_h > 0.003$	30 (±10)	50 (±10)	70 (±10)	85 (±10)	~ Ultimate	~ Ultimate

Notation:

w_{max} = maximum measured diagonal crack width (in.)

ρ_v = reinforcement ratio in vertical direction ($\rho_v = A_v / bs_v$)

ρ_h = reinforcement ratio in horizontal direction ($\rho_h = A_h / bs_h$)

A_v & A_h = total area of stirrups or horizontal bars in one spacing ($in.^2$)

s_v & s_h = spacing of stirrups or horizontal bars (in.)

b = width of web (in.)

Directions:

1). Determine ρ_v and ρ_h for bent cap

2). Measure maximum diagonal crack width, w_{max}, in inches

3). Use chart with w_{max}, ρ_v, and ρ_h to estimate % of capacity

Important Notes:

In this chart, the maximum width of the primary diagonal crack in a shear-critical member is linked to the load on the member, quantified as a percent of its ultimate capacity. The intent of this chart is to aide field engineers in evaluating residual capacity in diagonally-cracked, reinforced-concrete bent caps subjected to concentrated loads at a/d ratios between 1.0 and 2.0. This chart was developed from crack width data from 21 tests of simply-supported reinforced concrete beams with overall heights between 42" and 75". The testing was conducted at an a/d ratio of 1.85. Data has shown that diagonal crack widths may slightly decrease with decreasing a/d ratio. The same crack width at a smaller a/d ratio indicates that a higher percentage of capacity from the above chart has already been reached.

This chart should be used in conjunction with sound engineering judgement with consideration of the following limitations:

-variability in crack widths in general (± scatter)

-members loaded at a/d < 1.85 may be at slightly higher % of capacity

-differences between field and laboratory conditions

-implications of an unconservative estimate of capacity

This chart is not intended to be used for inverted-tee bent caps.

Figure 2-2: Chart linking diagonal crack width to load level (Birrcher et al., 2009)

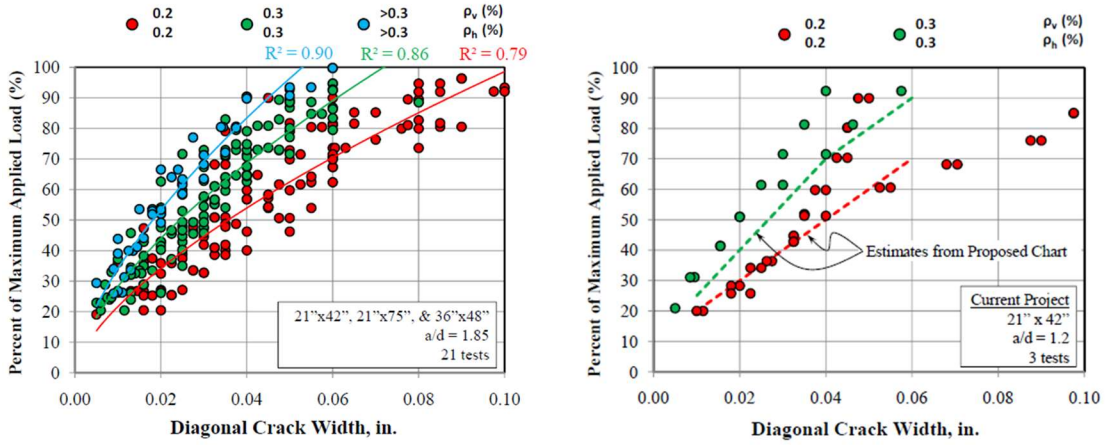

Figure 2-3: Development (left) and evaluation (right) of load level estimates in chart (adapted from Birrcher et al., 2009)

An alternative to using measured crack widths and spacings is to quantify crack patterns from images. Fractal analysis is a numerical procedure for classifying geometries which do not comply with typical Euclidean concepts and has been used to address many problems in image analysis (Lopes and Betrouni, 2009). Recently, researchers have utilized fractal and multifractal analysis (Ebrahimkhanlou et al., 2016; Farhidzadeh et al., 2013) to investigate crack patterns in RC shear walls. Changes in the fractal properties are empirically correlated to associated changes in the structure's behavior. Results from the RC shear walls showed good correlation between a proposed damage index and relative stiffness loss (Farhidzadeh et al., 2013). A statistics-based approach to crack pattern quantification has also been proposed (Kabir et al., 2009) which estimates the extent of damage based on acoustic borehole imagery. In both cases, accuracy can be affected both by the type of procedure or image processing used. Additionally, the ways these quantified damage patterns are correlated to mechanical properties of the structure are dependent on the method and/or element-type being investigated.

Many researchers in the past several decades have attempted to use Finite Element Analysis (FEA) techniques to estimate residual capacity of damaged RC elements. Techniques have varied from supplementing the analysis with fracture mechanics (Hillerborg et al., 1976; Sain and Kishen, 2007) to modelling initial damage discretely (Talley et al., 2014; Wang et al., 2013) to damage indices (Alembagheri and Ghaemian, 2013; Kono et al., 2006; Li et al., 2012; Park et al., 2001). All techniques have shown various levels of success; however, it should be noted that FEA can be time consuming and requires extensive experience to generate a model that accurately reflects structural behavior and to interpret the results from the analysis. Furthermore, RC is an inherently difficult material to model and there is no singular procedure or model which has been

shown to be universally acceptable for all situations encountered in practice (Vecchio, 2001).

Yet another approach to assessing damaged RC structures is concrete mechanics. Some researchers (Birrcher et al., 2009; Zhu et al., 2003) have proposed using strut-and-tie (STM) or compatibility-aided strut-and-tie models (CASTM) to correlate crack widths and applied shear forces. Birrcher et al. (2009) noted a problem with their STM-based approach: it was difficult to justify assumptions about the geometry of the bottle-shaped struts. The CASTM procedure, although it showed good agreement with experimental results – particularly in the service load level region, was calibrated with the same dataset it was assessed with. Therefore, more evidence is needed to support the notion that the procedure would offer similar performance for structural elements not included in the initial calibration.

Lantsoght et al. (2016) proposed another concrete mechanics-based model for the damage assessment of cracked RC elements. The underlying assumption of the method is that aggregate interlock accounts for all residual capacity in a cross section with a through crack. Equation 2-1 is the proposed model for the shear capacity of the cross section.

$$V_{agg} = \tau_u d b \qquad \textbf{Equation 2-1}$$

Where,

τ_u = $C_1(\rho f_y)^{C_2}$,
C_1 = $(f_c')^{0.36}$,
C_2 = $0.09(f_c')^{0.46}$,
ρ = reinforcement ratio,
f_y = yield stress of the reinforcement (N, mm),
f_c' = cube crushing strength of the concrete (N, mm),
d = effective depth of the considered cross section (mm),
b = width of the cross section (mm).

To correlate shear resistance with crack width, another approach based on Walraven's model for aggregate interlock (Walraven, 1980, 1981a, b) was proposed. In

this case, the cross section was assumed to be unreinforced. Note that, in both cases, the intent was to develop portions of a tiered approach with decreasing levels of conservativeness to be implemented in a codified procedure. The shear resistance-to-crack width relationship is shown in Equation 2-2.

$$V_{u_{unr}} = \tau b h \qquad \textbf{Equation 2-2}$$

Where,

$\tau = -\frac{f_c'}{30} + [1.8w^{-0.8} + (0.234w^{-0.707} + 20)f_c']\Delta$,
w = crack width (mm),
Δ = shear displacement (mm),
= $1.25w$ (for maximum aggregate size of 32 mm),
h = height of the cross section.

It is pertinent to note that this method has not been verified experimentally, but has only been compared to current Dutch design provisions (NEN 6720:1995).

Recent tests performed at the University of Toronto led to the development of a new crack behavior model (Calvi, 2015). Eighteen RC membrane (panel) elements were tested as a part of model development. These types of elements can represent many types of structural elements, such as a beam web. The model was developed to effectively analyze monotonic, cyclical, and reverse-cyclical loading scenarios using mechanics-based methods; however, it was also proposed that the model could be used to perform crack-based damage assessment of RC elements. It should be noted that there were two implicit assumptions included in the crack behavior model based on restrictions enforced in the experimental phase of the research: crack orientation and bond effects with longitudinal reinforcement. Cracks were forced to open perpendicular to applied tension and parallel to applied shear by casting steel wedges in place with the panels which functioned as "crack initiators." Bond effects were eliminated using plastic tubes around longitudinal reinforcement to reduce dowel action resistance at crack locations. These built-in

assumptions simplified equilibrium equations and reduced uncertainty about bond relationships with crack width and slip (Calvi, 2015). The RC panel test setup is shown in Figure 2-4.

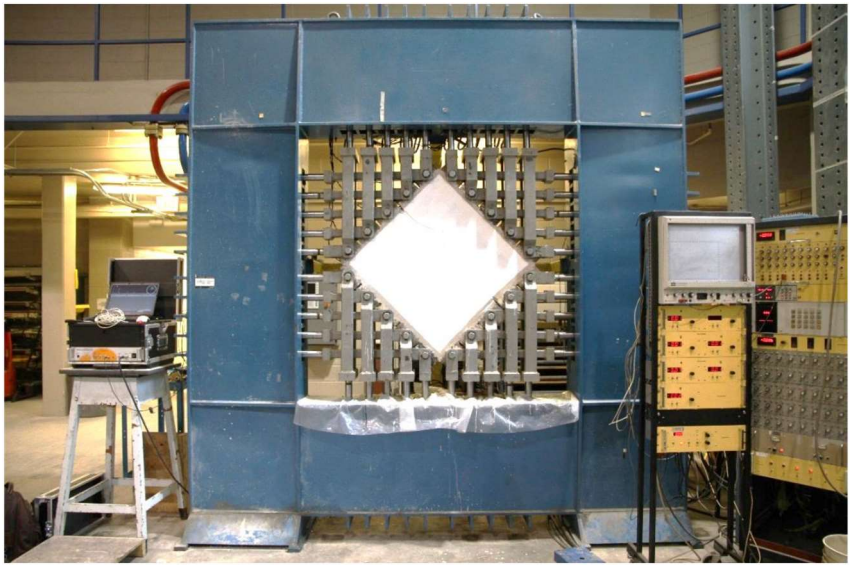

Figure 2-4: Panel test setup (Calvi, 2015)

The model is referred to as the Assessment of Cracked Reinforced Concrete (ACRC) model. The ACRC equations are summarized in Figure 2-5. By solving these equations, one can obtain estimates of reserve capacity for concrete crushing, reinforcement yielding, and aggregate interlock. Additionally, a global reserve capacity can be calculated by estimating shear resistance with a non-linear RC model and comparing the computed shear for a given crack width to the ultimate shear capacity of the element. It is pertinent to mention that the model can handle many different crack inputs, such as crack width, slip, inclination, and spacing. Note that crack width and inclination are perhaps the most critical measurements; however, the model prefers knowledge of crack slip. If crack slip is not known, it is assumed to be zero. Crack spacing can be estimated

with any available procedure if it cannot be easily measured. Another required input is loading proportions between the x-direction and shear as well as y-direction and shear.

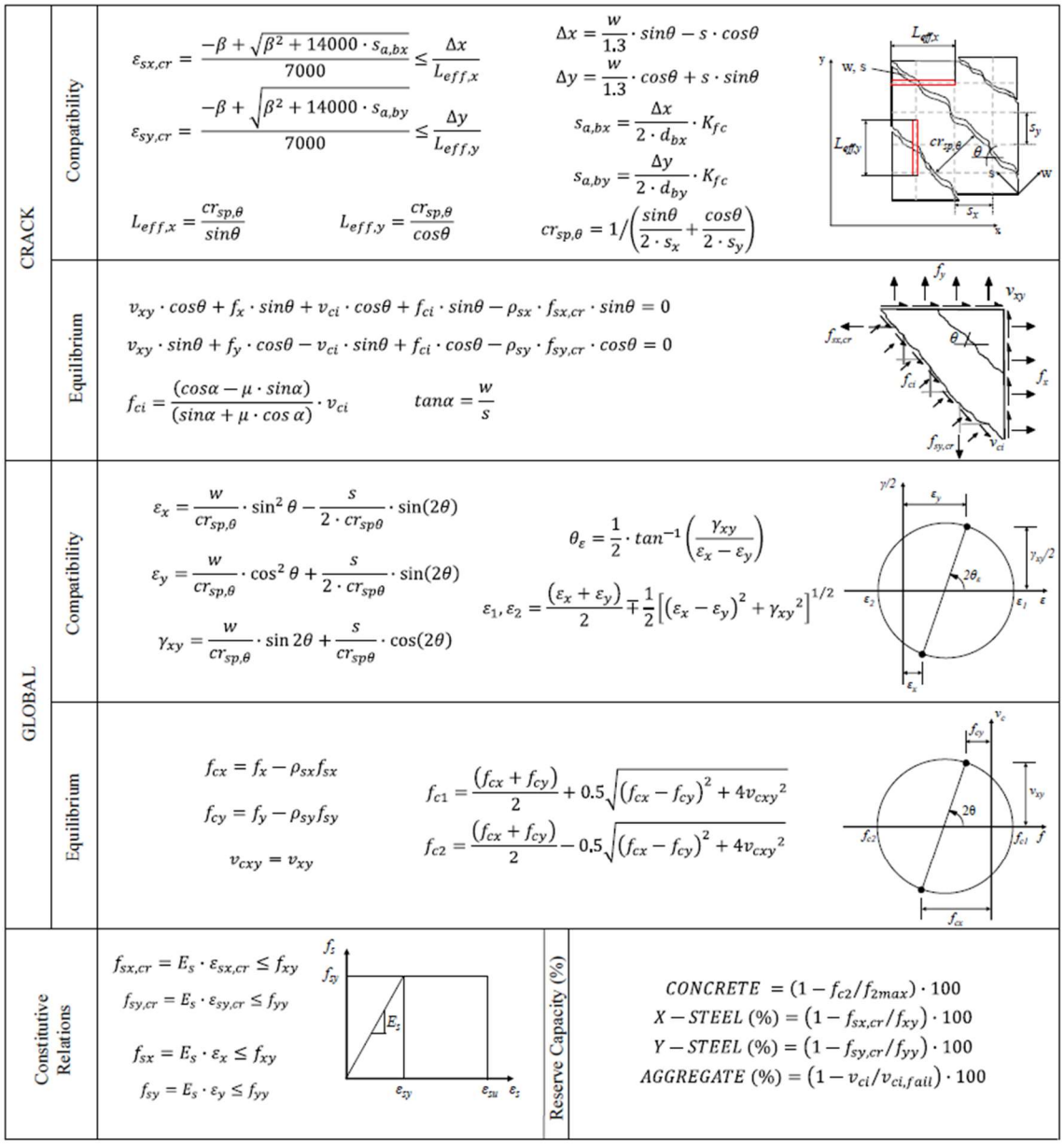

Figure 2-5: Equations of the ACRC model (Calvi, 2015)

The ACRC was validated with two panel element test series (Proestos et al., 2015; Ruggiero et al., 2014), as well as three slender beams tested by Higgins et al. (2004).

Estimated results for shear force compared well with measured values, as did residual capacity estimations. Calvi (2015) observed larger amounts of conservatism at low load levels, where residual capacity is higher. Overall, the model performed well, but requires more experimental validation for the crack-based assessment of beams.

2.3 DISCUSSION

The methods currently employed in practice to evaluate RC structures are practical regarding their ability to recommend action based on visually inspected damage without the use of overly complicated or costly tools. Additionally, these methods are typically simple to implement as they usually require little input and the output is straightforward with clear guidelines for remedial action. Furthermore, these methods are well established and have been used for several decades; as such, there is a level of comfort and trust in their use. However, the quality of the observations and results from current methods are highly dependent on the individual inspector's experience. Additionally, these methods typically provide little information on the calculation of residual structural capacity. These two factors may lead to rehabilitation money being prioritized for bridges that are only marginally structurally inadequate while others that have suffered damage more likely to significantly reduce a bridge's capacity may be deemed lower priority or may potentially be insufficiently rehabilitated.

Current methods for estimating the residual capacity of a cracked RC element are varied in their approach and success. Generally, methods which rely on visual rating systems (Abi Shdid et al., 2006; Gulkan & Yakut, 1996; Melchor-Lucero & Ferregut, 1996; Paal et al., 2015; Veletzos et al., 2008) offer mixed performance or are limited to specific structural elements or load types. Empirically derived approaches (Birrcher et al., 2009; Larson et al., 2013) are highly practical, but are limited in their generality. Image-based,

crack quantification style procedures (Ebrahimkhanlou et al., 2016; Farhidzadeh et al., 2013; Kabir et al., 2009) generally require the structure's history to be known and may function better as long-term monitoring or supplementary assessment tools. FEA has been shown to work in a variety of procedures (Alembagheri and Ghaemian, 2013; Hillerborg et al., 1976; Kono et al., 2006; Li et al. 2012; Park et al., 2001; Sain and Kishen, 2007; Talley et al., 2014; Wang et al., 2013) and is general in its application, but requires a high-level of experience and time to use effectively. Mechanics-based procedures on the other hand (Birrcher et al., 2009; Calvi, 2015; Lantsoght et al., 2016; Zhu et al., 2003), tend to be much simpler than FEA procedures but retain much of the generality. However, very few extensively experimentally verified mechanics-based procedures exist which constitutes a gap in the current literature. To allow for wider experimental verification, a visual crack measurement database has been compiled and discussed in Chapter 3 and in the supplementary file "VCMD." Furthermore, Chapter 4 presents the foundation and appraisal of a preliminary crack-based assessment method using the MCFT as a base.

Chapter 3: Visual Crack Measurement Database

This chapter includes four sections focused on the creation and use of a Visual Crack Measurement Database (VCMD). The first section provides a brief discussion of the data comprising the VCMD. The next section discusses the organization, functions, and applications of the VCMD. The third section presents some trends identified from the data and the chapter concludes with discussion of the VCMD.

3.1 Data Comprising the Visual Crack Measurement Database

Data from ten experimental programs was used to populate the VCMD resulting in a total of 155 RC members with 943 crack measurements at load levels ranging from 10 % to approximately 100 % of ultimate. Crack measurements constitute maximum diagonal crack widths and/or inclinations, depending on availability in the literature. Generally, it was sought to document maximum diagonal crack widths with associated inclinations; however, crack widths were typically well-recorded over a larger variety of load levels than inclinations were leading to load level entries without inclination measurements. Reported values were normally used in the VCMD, apart from inclinations estimated from crack patterns where there were no reported values. A summary of the data comprising the VCMD is presented in Table 3-1.

Potential test data for the VCMD were collected during the literature review summarized in Chapter 2. In collecting data, emphasis was placed on collecting data pertaining to beams which were relevant in either detail or scale to typical RC bridge members identified in the field data review in Chapter 1. Beams with large effective depths (e.g., greater than 24 in.) were preferred, which is consistent with depths of in-service members. An example of a typical beam member comprising the VCMD is shown in Figure 3-1.

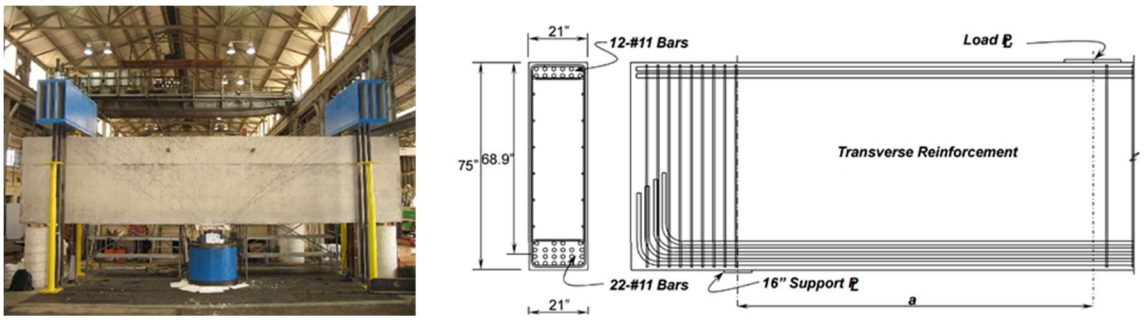

Figure 3-1: Test setup (left); specimen cross section and rebar layout (right) (adapted from Birrcher et al., 2009)

Although a large volume of data was collected, not all data were useful in the context of a visual crack measurement database for traditional RC beams failing in shear. First, the emphasis of the procedure detailed in Chapter 4 is for traditional reinforcement; thus, prestressed specimens were not included in the VCMD. Members that failed by flexure-governed behavior were omitted from the database since the emphasis was on diagonal cracking and shear-governed failures. Furthermore, some seemingly relevant studies documented highly-specialized diagonal cracking (e.g., cracking at reentrant corners of inverted T-section ledges) which is not generally typical to RC infrastructure. These test programs were considered out-of-scope for the VCMD and characteristically different than the diagonal web cracking reported for the other members.

Table 3-1: Data comprising the VCMD

Source	Member Type	No. of Tests
Birrcher et al. (2009)	Rectangular	35
Bracci et al. (2000)	Rectangular	16
Larson et al. (2013)	Inverted T	26
Aguilar (2011)	I-Girder	8
De Silva et al. (2008)	I-Girder	3
Pang (1991)	Panel	10
Sherwood (2008)	Rectangular	35
Susetyo (2009)	Panel	2
Lee et al. (2015)	Rectangular	12
Yoon et al. (1996)	Rectangular	9

3.2 VISUAL CRACK MEASUREMENT DATABASE

The VCMD is accessible in a macro-enabled Microsoft Excel (MS-Excel) worksheet and contains many features which are convenient for the assessment of diagonally-cracked RC beams and for the development of numerical procedures. The following section describes the organization, functionality, and potential application of the VCMD. The VCMD is available in PDF form as the supplementary file "VCMD."

3.2.1 Organization

A category system was used to sort data by relevance for the damage assessment of RC bridge members. The organization of the VCMD entries reflects data categories, followed by additional sorting based on alphabetical order. In general, members were organized within a source the same way they were presented in the literature. Each member and entry were assigned a member or entry number, respectively, to assist in tracking the

data logged in the VCMD and to standardize entries from different sources. There were five subdivisions on entries in the VCMD, as follows:

- *'Member information*' includes source name and member name provided within the source.
- *'Geometric properties*' includes the dimensional classification of the member.
    - Web width (in.): width of web or "web equivalent." For example, in a panel element test (Pang, 1991; Susetyo, 2009), the panel thickness was taken as the width.
    - Total height (in.): total height of specimen.
    - Effective depth (in.): depth from compressive surface to the centroid of the tensile reinforcement.
    - Shear span-to-depth ratio: ratio between shear span and effective depth. Shear span is given as the distance between the applied point load and the support point.
    - Clear cover (in.): distance between nearest face and reinforcement in that region of specimen.
- *'Reinforcement details'* contains reinforcement bar information.
    - Reinforcement ratio (%): ratio between area of steel and area of concrete. Calculation varies based on location of steel (top, bottom, side, etc.).
    - Number of bars: number of bars for each reinforcement type (e.g., tension, compression, shear, and skin reinforcement).
    - Bar diameter (in.): bar diameters corresponding to the respective bar types noted above (refer to 'Number of bars').
    - Bar spacing (in.): maximum spacing for a group of bars/bar type.

- Concrete and steel materials strength are recorded in the '*material properties'* section.
    - Concrete compressive strength (psi): traditional concrete cylinder compression strength.
    - Maximum aggregate size (in.): maximum nominal coarse aggregate size specified in mix design.
    - Steel yield strength (ksi): traditional steel yield strength.
- The visual crack measurements and related information are recorded in the *'crack data*' section.
    - Shear loads – cracking and failure (kips): shear cracking loads recorded where applicable, otherwise only failure shear load was recorded.
    - Maximum (characteristic) crack width (in.): the maximum diagonal crack width recorded on the specimen for a given load stage.
    - Crack inclination (degrees): crack inclination at mid-depth of member, approximately halfway between load and support points and representing the angle between the longitudinal axis and the inclined crack.

3.2.2 Functions

There are several features built-in to the MS-Excel formatted database that can be used to easily navigate or access specific data. Current built-in features include: data filtering, report generation, and automatic crack information plotting. It is envisioned that the VCMD will be a "living database" that will be updated to incorporate additional data, as it becomes available, and additional features for the usage of the VCMD.

The first key feature and benefit to using the electronic version of the database is filtering. Each of the entry types listed in Section 3.2.1 can be filtered using various criteria.

A dropdown menu is shown when the filter icon is clicked and the user can manually check or uncheck certain criteria based on what type of specimen users would like to access. For example, if the user was interested in comparing the cracking behaviors of members with rectangular cross sections ranging from 48 to 70 in., it simply requires applying filters to the shape and effective depth columns. In this way, the user can quickly focus attention on parameters of interest, rather than manually sifting through a lengthy database.

If the user wants a quick look at a specific member, or to save those results for convenient viewing later, the "Report" tab of the electronic database can be used. The report tab utilizes two drop down menus which allow for quick filtration of data. First, simply select a source from the source list. Next, choose a member from the subsequent dropdown menu labeled "member." The second selection will automatically populate the rest of the report sheet with data from the database. These results can be printed or exported for the user's convenience.

Another product of the report tab is plot generation. There are three default plots included in this version of the database: crack width-load level, crack inclination-load level, and crack width-crack inclination. These plots are updated in tandem with the rest of the report page, and can be printed alongside the rest of the report for convenience. A sample report with associated figures is attached in the "VCMD" supplementary document.

3.2.3 VCMD Application

The previous section covered some of the built-in functions within the electronic version of the database, while this section will discuss potential uses for the database. It is envisioned that the electronic version of the database will have four primary uses:

- Developing new crack-based shear strength assessment procedures
- Evaluating new and existing crack-based shear strength assessment procedures

- Providing visual benchmarks for field data
- Serving as a resource for future projects focused on related research areas

The database was used in the development and evaluation of the mechanics-based procedure detailed in Chapter 4. Additionally, it is envisioned that existing procedures which have not been extensively vetted against experimental data (Calvi, 2015; Lantstoght et al., 2016) could potentially benefit from further verification using the VCMD.

This database can also provide functions like the ODOT (2009) *Bridge Inspection Pocket Coding Guide*. There are several different member shapes and sizes recorded at a variety of different reinforcement ratios and concrete strengths over several load levels. Using the filtering features to isolate the data relevant for a given bridge member under inspection, an inspector could use the database as an additional tool to evaluate the extent of damage from visual structural cracking.

Finally, there is a wealth of information stored within this database that will ideally serve future researchers in related endeavors. As research continues to advance in the assessment of visually observed damage in RC infrastructure, it is anticipated that this database will grow and continue to assist researchers and practitioners alike.

3.3 VCMD TRENDS

A general overview of the maximum crack widths and their associated load levels are shown in Figure 3-2. Clearly, there are essentially no visible trends in the whole dataset; however, a few key parameters were isolated to investigate potential trends within the VCMD. These parameters were shear span-to-depth ratio, effective depth, and web reinforcement ratios (shear and skin). Figure 3-3 shows the relationship between normalized load level and maximum measured diagonal crack width for shear span-to-

depth ratio and effective depth bands. Figure 3-4 shows the influence of reinforcement ratios on maximum crack width.

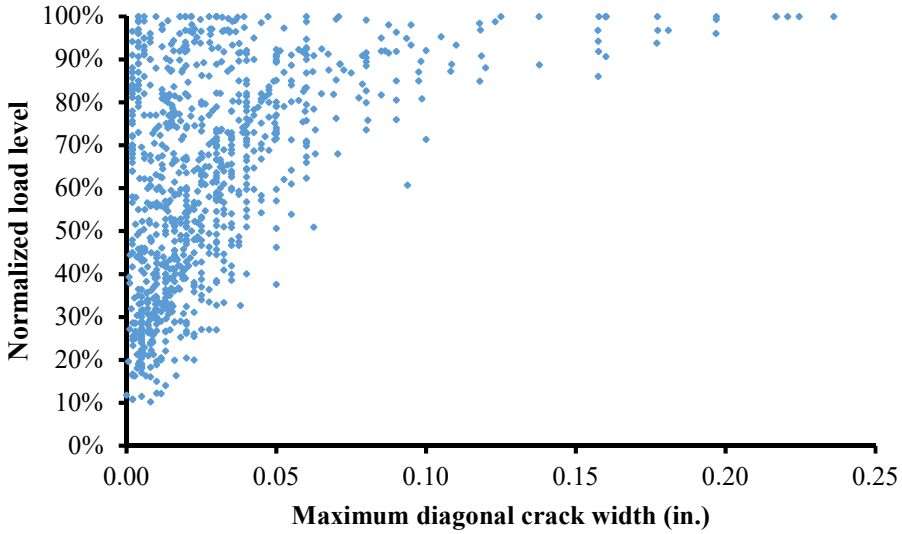

Figure 3-2: Overview of VCMD data

It is difficult to ascertain any clear trends based on shear span-to-depth ratio, despite the role it plays in beam behavior. While there are some clear bands of data points from bent cap projects (Birrcher et al., 2009; Larson et al., 2013) where empirical curves may fit; there is still a large amount of overlap and no clear separation in data trends based on shear span-to-depth ratio alone. This is consistent with findings from previous studies correlating crack widths to residual capacities in bent caps (Birrcher et al., 2009; Larson et al., 2013), which found that crack width was not particularly sensitive to shear span-to-depth ratio.

The effective depth plot shows much clearer trends. That is, members with larger effective depths exhibited much larger maximum crack widths due to size effect in RC. This suggests that the inclusion of size-related effects may be a critical factor in the assessment of in-service beams. If one were to simply try and correlate crack measurements

and load levels from small scale experiments, a significant amount of error would likely be introduced into the predictions. However, it should also be noted again that there is variability in the data due to the stochastic nature of cracking.

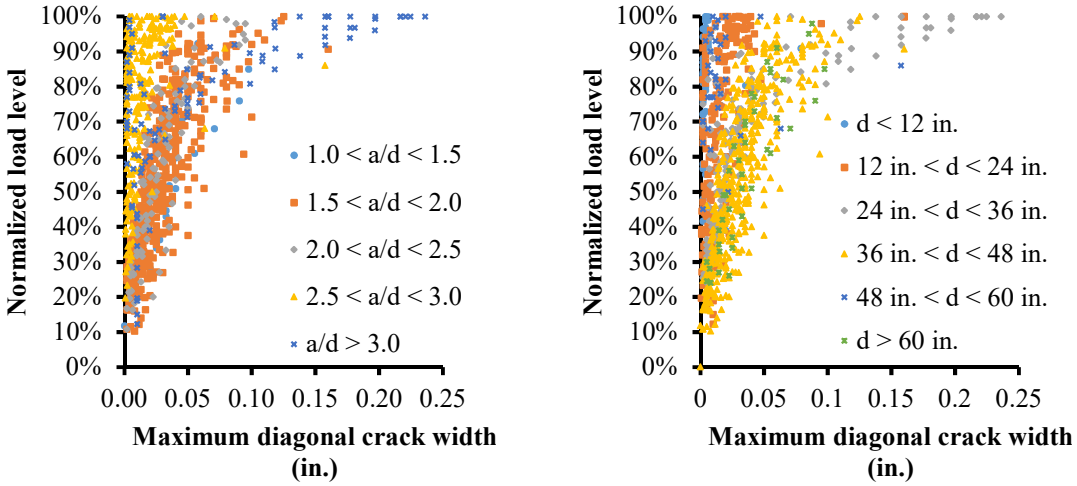

Figure 3-3: Influence of shear span-to-depth ratio (right) and effective depth (left) on maximum crack width

Lastly, the influence of web reinforcement ratios was investigated. The reinforcement ratios are calculated as the ratio of reinforcement area per layer (A_s) to the product of web width (b_w) and bar spacing (s_b) for shear reinforcement ($\rho_v = A_{sv}/b_w \cdot s_{bv}$) and skin reinforcement ($\rho_h = A_{sh}/b_w \cdot s_{bh}$). Beams containing greater than 0.20 % reinforcement in both directions exhibited closer grouping than those with less than 0.20 %. Although the limited number of tests is contributing, at least in part, to this grouping, it is also being caused by the web reinforcement limiting crack widths. Furthermore, it appears from the beams in the VCMD that once minimum web reinforcement is provided, additional reinforcement has a modest effect on maximum crack widths. However, it is clear from Figure 3-4 that reinforcement detailing will be a significant contributor to the accuracy of crack-based assessment in RC.

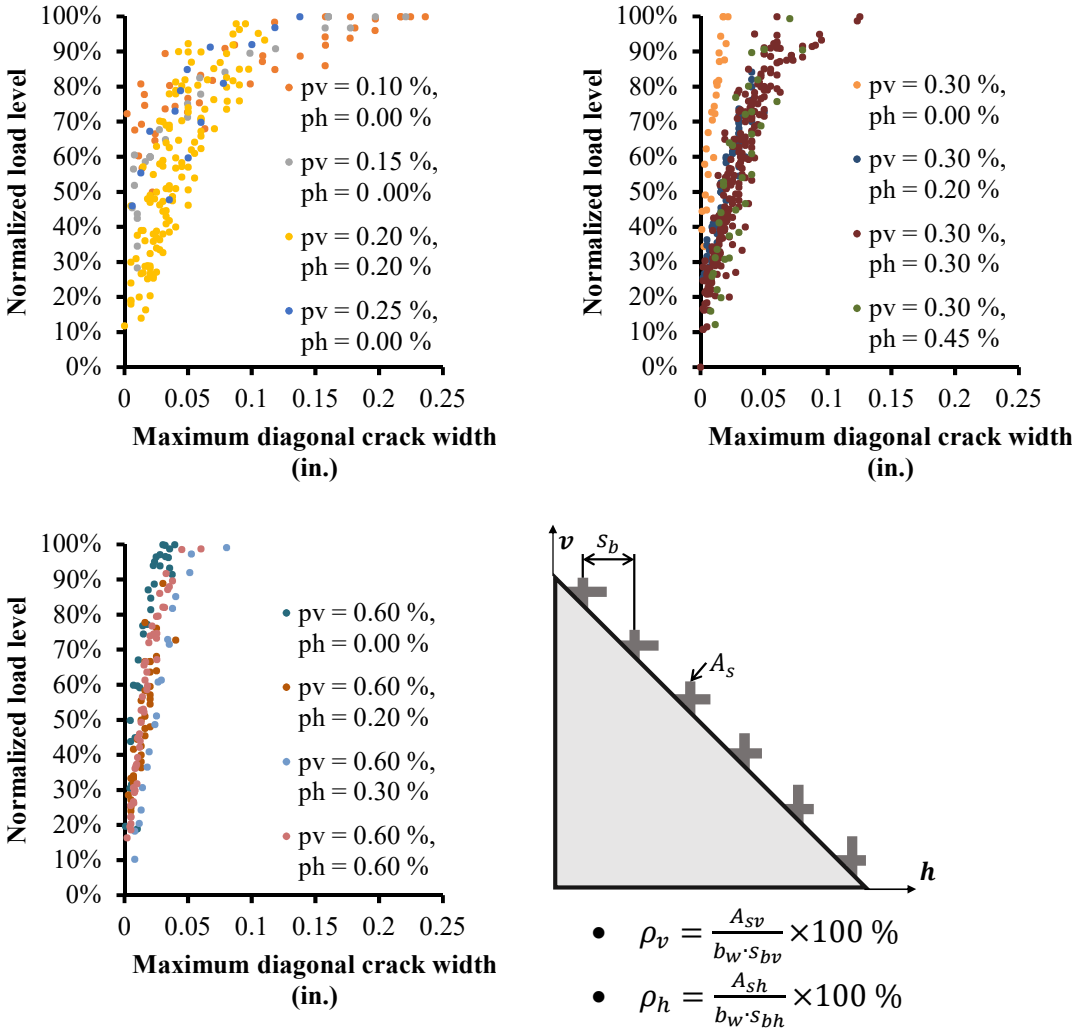

Figure 3-4: Influence of reinforcement ratio on maximum crack width

3.4 DISCUSSION

This chapter detailed the creation and use of the VCMD including the data within the database, the organization, function, and use of the database, and a brief investigation into trends in the data. The MS-Excel VCMD is envisioned to be a convenient and easy tool for users interested in benchmarking visual crack measurements, evaluating assessment procedures, and developing new procedures for the visual assessment of RC beams. Trends in the data call for careful consideration of the many variables at play in the

shear assessment of damaged RC beams as not all cracks are ‘equivalent.’ As seen in the Figure 3-2, a crack width of 0.05 in. can be indicative of anything from 60 to 0 % residual capacity left in a beam. Important variables, such as depth effect and reinforcement ratios, must be included in the development of crack-based assessment procedures for them to remain applicable to the wide variety of in-service structures.

Chapter 4: Mechanics-Based Crack Assessment

This chapter lays out the foundation of a mechanics-based crack assessment procedure which has been developed. The first section of the chapter includes compatibility relationships, constitutive laws, equilibrium equations, and additional assumptions required for the analysis. The second section presents a preliminary procedure for crack-based assessment of RC bridge members. The third section presents the results from a series of analyses performed using the proposed procedure. Lastly, there is a discussion section to finish the chapter.

4.1 PROCEDURE FOUNDATION

This section provides a brief overview of the foundation of the procedure which includes a discussion of crack spacing models, the modified compression field theory (MCFT), and disturbed region influence on RC member damage assessment.

4.1.1 Crack Spacing and Width Models

Many models have been developed to estimate crack spacings and widths and are useful for mechanics-based crack assessment procedures. Crack spacing and width in RC has been shown to be directly related to the slip between concrete and embedded reinforcing steel (CEB-FIP, 1990). Figure 4-1 shows estimated stress distributions along the length of a RC member under uniaxial tension. Across the width of a crack, the concrete stress is assumed to be zero and, as a result, reinforcement must carry the entire tensile load. However, within the uncracked regions of the concrete, the sound concrete can still develop tensile stress. Since the crack spacing and width are related by slip, average elongation (i.e., strains averaged over both cracked and uncracked sections) perpendicular to cracks is generally associated with changes in crack width.

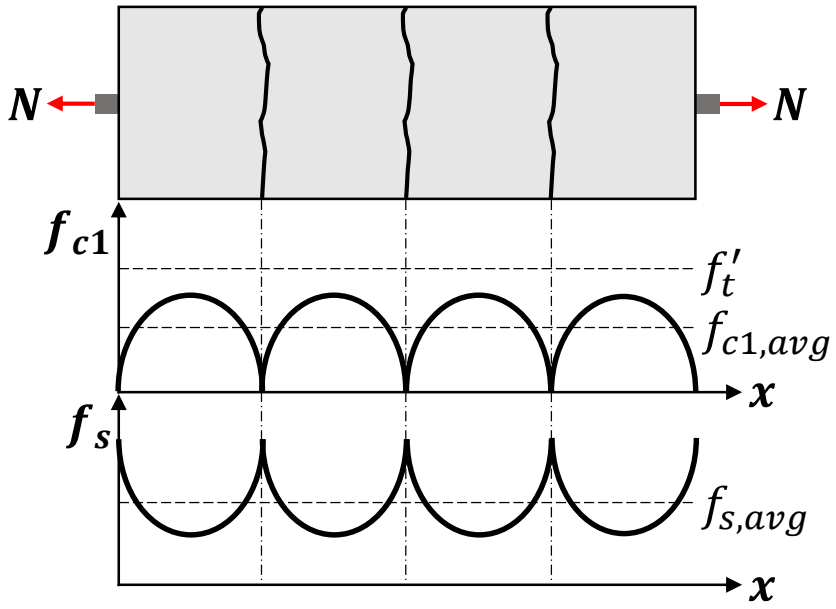

Figure 4-1: Average concrete and steel stresses in cracked RC (adapted from CEB-FIP 1990)

For the purposes of a crack-based assessment procedure, crack widths can be measured but, as shown in the field data review (Section 1.2), deep beams often exhibit moderate-to-severe cracking in the form of only a few localized cracks. Where few cracks exist, it can be difficult to measure crack spacing accurately (e.g., how does one measure the average crack spacing from a single crack?) and the implementation of a crack spacing model may be more appropriate and suitable for the application of mechanics-based procedures. An important note regarding the crack spacing models presented herein is that nearly all the models assume the concrete is loaded under uniaxial loading conditions. Crack spacing characteristics for multiaxial loading conditions that are not transverse to the primary reinforcement are usually calculated using various supplementary procedures (see Figure 4-3) using a combination of crack spacing estimates computed in individual reinforcement directions.

The assumption inherent to the uniaxial loading condition formulation is that crack orientation typically coincides with principal stress orientation, since cracks are most likely

to form perpendicularly to the principal tensile stress. On that basis, measured crack inclinations can be used to estimate the orientation of the principle stress and strain fields for in-service RC members.

The application of crack spacing models in the context of providing a quantitative analysis of a damaged RC member lies in the aforementioned relationships. Several models for the calculation of crack spacing and width have been developed and refined over the past half century. Calculated crack widths, spacings, and inclinations are all dependent on the stress-strain state of the member; however, the actual cracking process is random and therefore can be very difficult to predict. As such, there is typically a relatively wide scatter between the predicted data and the experimental data used for verification. Although there are several generally accepted methods that have been shown to be relatively accurate, there is still little agreement on a single model that can be used to predict cracking conditions at various load levels (Chowdhury and Loo, 2001). Furthermore, studies have shown that a cracking model's accuracy can depend greatly on the type of member being investigated (Xiang et al., 2012). A brief overview of sample crack spacing and width models is presented in sections 4.1.1.1 through 4.1.1.3.

Prior to the introduction of any specific model, some commonalities will be discussed. Crack spacing models can be generally employed to estimate either mean or maximum crack widths; furthermore, these models often use a factor to convert between the two. Equation 2-1 shows this relationship for maximum (subscript '*k*') and mean (subscript '*m*') crack spacing, where the conversion factor is given as 'β.' Typically this coefficient varies between 1.3 and 1.7 depending on the model and the experimental data being investigated (Chowdhury and Loo, 2001). Mean strain across the average section (cracked and uncracked) is given by Equation 4-2, the ratio of crack width to crack spacing. Typically, the way mean strain is estimated is based on the model being used and Equation

4-2 is rearranged to provide an estimate of crack width. However, in the mechanics-based crack assessment procedure presented in this chapter, Equation 4-2 is used as shown with measured crack widths (w_m) and measured or estimated crack spacing (s_m) to estimate mean principal tensile strain. This has been shown to provide reasonable estimates in many existing mechanics-based analysis procedures (Vecchio and Collins, 1986; Vecchio, 2000; Calvi, 2015; etc.). As such, additional discussion on mean strain calculations based on codified expressions is not provided.

$$s_k = \beta s_m \qquad \textbf{Equation 4-1}$$

$$\varepsilon_m = \frac{w_m}{s_m} \qquad \textbf{Equation 4-2}$$

4.1.1.1 CEB-FIP/fib

The European Committee for Concrete and International Federation for Prestressing (CEB-FIP), now known collectively as the International Federation for Structural Concrete (*fib*), is a European based committee that has developed model codes since the late 1970s. Thus far, three codes have been published: the 1978, 1990 and 2010 Model Codes. Each iteration has provided an updated method for the calculation of concrete crack spacing and crack widths. The Model Code 1978 calculates mean crack spacing using Equation 4-3. There were no updates to crack spacing between Model Codes 1990 and 2010, both versions are shown in Equation 4-4.

$$s_m = 2\left(c_c + \frac{s_b}{10}\right) + k_1 k_2 \frac{d_b}{\rho} \qquad \textbf{Equation 4-3}$$

$$s_k = \frac{d_b}{3.6\rho} \qquad \textbf{Equation 4-4}$$

Where,
c_c = concrete clear cover,
s_b = reinforcement spacing,
k_1 = 0.4 for deformed bars,
= 0.8 for plain bars and prestressing strands,

k_2 = 0.125 for bending,
= 0.25 for tension,
= $0.125\frac{(\varepsilon_1+\varepsilon_2)}{\varepsilon_1}$ for cases of eccentric tension or web regions of beams,
d_b = reinforcement diameter,
ρ = reinforcement ratio.

4.1.1.2 Deluce, Lee and Vecchio (2014)

After a series of experimental programs examining the behavior of fiber-reinforced concrete (FRC) members containing conventional reinforcement, Deluce et al. (2014) concluded that there was a lack of accurate models available for predicting the cracking behavior of FRC. The Model Code 1978 was selected as a base model which was then modified appropriately to account for fiber-reinforcement. The most salient change, within the context of using crack spacing and width models with a mechanics-based approach to damage assessment of traditional RC members, is the way biaxial stress conditions were handled. All other models discussed in this report assume an x, y, z coordinate system, shown in Figure 4-2, based on traditionally used primary reinforcement directions; however, this model uses a coordinate system based on the directions of the principal axes of stress instead. This allows for more convenient and accurate classification of cracking behavior for reinforcement which is not orthogonal to an x, y, z coordinate system. Equation 4-5 summarizes the portion of the model which is applicable to conventional RC members.

$$s_m = 2\left(c_a + \frac{s_{b1}}{10}\right) + \frac{k_1 k_2}{s_{mi1}} \qquad \textbf{Equation 4-5}$$

Where,
c_a = effective concrete cover which can be taken as 1.5 times maximum aggregate size,
s_{b1} = effective longitudinal bar spacing in principal tensile direction,
= $\left(\sum_i \frac{4\rho_i}{\pi d_{b_i}^2}\cos^4\theta_i\right)^{-\frac{1}{2}}$,
θ_i = angle between the i^{th} reinforcement layer and the principal tensile axis,

s_{mi1} i^{th} reinforcement effectiveness parameter in the principal tensile direction,

$= \sum_i \frac{\rho_i}{d_{b_i}} \cos^2 \theta_i$,

Other quantities are as given in Section 4.1.1.1.

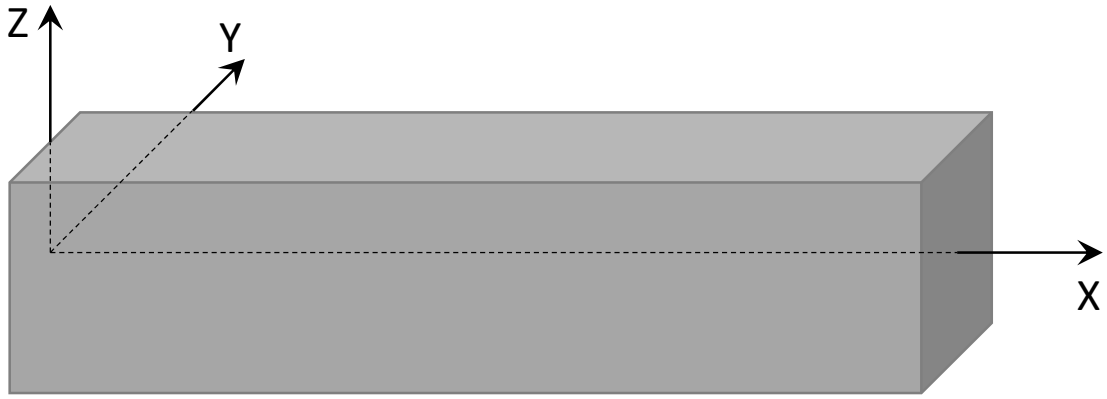

Figure 4-2: Typical x, y, z coordinate system for a beam

4.1.1.3 Eurocode 2

Eurocode 2 is the European standard for RC design provisions. The original 1991 edition was updated in 2003. Both editions contain crack width and spacing formulations like the CEB-FIP 1978 Model Code. The 1991 edition of the Eurocode 2 (European Committee for Standardization, 1991) provides an expression for calculating mean crack spacing (Equation 4-6) using input of millimeters. The 2003 edition of Eurocode 2 (European Committee for Standardization, 2004), provides a similar formulation, but it employs a maximum crack spacing, rather than mean crack spacing. The maximum crack spacing is given by Equation 4-7. Note that the equation is now given in a more dimensionally indistinct form, so input is no longer restricted to units of millimeters.

$$s_m = 50 + 0.25 k_1 k_2 \frac{d_b}{\rho} \qquad \textbf{Equation 4-6}$$

Where,

k_1 = 1.0 for deformed bars,

= 0.5 for plain bars and prestressing strands,

k_2 = 0.5 for bending,

$=$ 1.0 for tension,
$=$ $\frac{\varepsilon_1+\varepsilon_2}{2\varepsilon_1}$ for eccentric tension or web regions of beams.

$$s_k = k_3 c_c + k_1 k_2 k_4 \frac{d_b}{\rho}$$ **Equation 4-7**

Where,
k_1 $=$ 0.8 for deformed bars,
$=$ 1.6 for plain bars,
k_2 $=$ 0.5 for bending,
$=$ 1.0 for tension,
$=$ $\frac{\varepsilon_1+\varepsilon_2}{2\varepsilon_1}$ for cases of eccentric tension or web regions of beams,
k_3 $=$ 3.4 for general case,
k_4 $=$ 0.425 for general case.

4.1.1.4 Discussion and Model Selection

It is clear from the models presented in this section that there are several key parameters which influence crack spacing. All the above models identify reinforcement ratio and diameter as being important variables in estimating crack spacing. Depending on the complexity of the model, additional reinforcement characteristics (e.g., clear cover, bar spacing, and bar deformations) may or may not be included. Furthermore, some models include the influence of the loading conditions.

For the procedure presented herein, the CEB-FIP 1978 crack spacing model was selected. It does not carry any dimensional dependence, which is convenient, and includes all important variables identified by the models. Additionally, it is the model that was used in the first iteration of the MCFT (Vecchio and Collins, 1986) and is still the default model used in the nonlinear finite element analysis software VecTor2 which uses the MCFT/ DSFM as a base (Wong et al., 2013). Therefore, its selection is consistent with any built-in assumptions in the rest of the procedure, since the MCFT forms the backbone of the procedure. In more complex reinforcement layouts, it may be prudent to switch to the alternate 1978 model proposed by Deluce et al. (2014); however, the beams in the VCMD

are all reinforced orthogonally in the x- and y-axes and do not necessarily benefit from the alternate formulation.

4.1.2 Modified Compression Field Theory (MCFT)

The MCFT is a smeared, fully-rotating crack model for predicting the response of RC elements based on average stress-strain relations (Vecchio and Collins, 1986). The MCFT forms the backbone of the modeling procedure presented herein. The MCFT introduced three important concepts for the analysis of cracked RC: tension stiffening, compression softening, and examination of local (i.e., at the crack) stress conditions. Tension stiffening is a constitutive phenomenon through which the concrete component in RC can continue to carry tensile stresses after cracking. Compression softening describes a reduction in concrete compressive strength and stiffness in the presence of transverse tensile strain. The examination of local crack stresses involves equilibrium checks which ensure that the reinforcement can develop localized increases in principal tension across the crack interfaces because of tension stiffening. Furthermore, it checks that the aggregate interlock capacity of the crack interface is not exceeded by the resultant crack shear stress equilibrating the local increase in steel stress. These phenomena are dependent on principal tensile strain which is being estimated in this procedure using crack widths as described in Section 4.1.1. In addition to other assumptions made specifically for the crack assessment procedure, the following assumptions are inherent to the original 1986 MCFT procedure: uniformly distributed reinforcement, uniformly applied stresses, perfect bond between concrete and reinforcement, smeared (evenly distributed) cracking, and coincident principal stress and strain directions (no crack slip).

To simplify the problem of assessing a damaged RC member with unknown loading conditions, a single, averaged element will be considered. The single, averaged element

approach has been shown to provide adequate estimates of beam web shear strength (Bentz et al., 2006). Due to this assumption, discrete reinforcement layers (such as the primary tensile longitudinal reinforcement comprising a beam-type member) are not explicitly considered as lumped reinforcement. Rather, concentrated reinforcement is treated as being evenly distributed over depth '*d*,' which ensures the following items are accounted for: tension stiffening effects, average normal stresses induced by bending-action, and additional strengthening/stiffening from inclusion of the lumped reinforcement.

The MCFT uses equations of compatibility, constitutive models, and equilibrium to estimate member response stemming from some 2-dimensional state of stress. However, in the proposed crack-based assessment procedure, the solution process will be inverted. Beginning with a damage pattern (i.e., crack width, crack inclination, and crack spacing), a state of stress is estimated and used to correlate visually observed damage to structural health. The basic set of equations from the MCFT suited for this application is summarized in Figure 4-3. Note that local stresses may be transformed with a Mohr's Circle of Stress, like the equations given for average strains, but have been omitted from the figure for brevity. Additional resources regarding derivations, equations, and alternative solution procedures are available in the literature (Bentz et al., 2006; Vecchio and Collins, 1986; Vecchio, 2000).

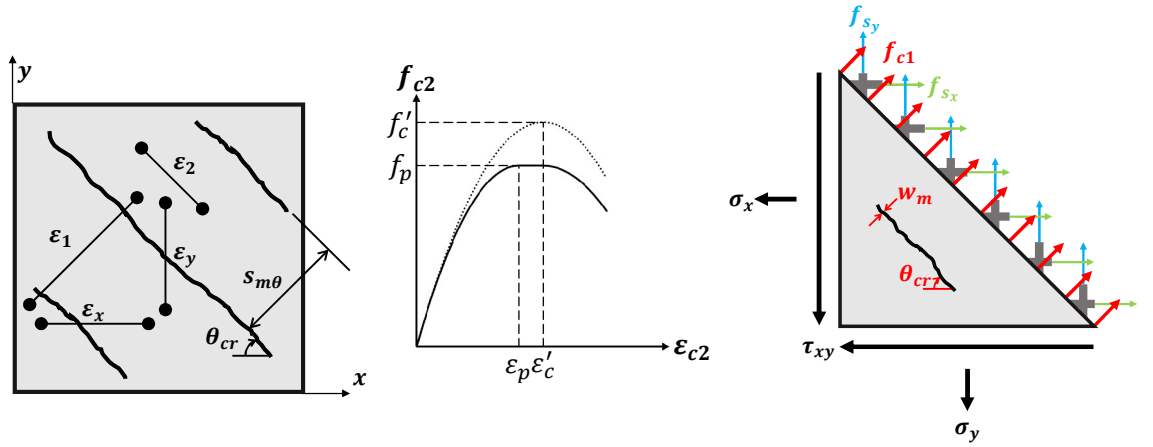

Geometric Conditions:	***Constitutive:***	***Equilibrium:***
Compatibility: $\varepsilon_x = \varepsilon_{cx} = \varepsilon_{sx}$ $\varepsilon_y = \varepsilon_{cy} = \varepsilon_{sx}$ **Average Strains:** $\varepsilon_{cx} = \varepsilon_{c1}\sin^2\theta_{cr} + \varepsilon_{c2}\cos^2\theta_{cr}$ $\varepsilon_{cy} = \varepsilon_{c1}\cos^2\theta_{cr} + \varepsilon_{c2}\sin^2\theta_{cr}$ $\gamma_{cxy} = (\varepsilon_{c1} - \varepsilon_{c2})\sin 2\theta_{cr}$ **Crack Conditions:** $w_m = \varepsilon_{c1} s_{m\theta}$ $s_{m\theta} = \left(\frac{\sin\theta_{cr}}{s_{mx}} + \frac{\cos\theta_{cr}}{s_{my}}\right)^{-1}$	**Concrete:** $f_{c1} = \frac{f'_t}{1 + \sqrt{C_t \varepsilon_{c1}}}$ $f_{c2} = -f_p\left[2\left(\frac{\varepsilon_{c2}}{\varepsilon_p}\right) - \left(\frac{\varepsilon_{c2}}{\varepsilon_p}\right)^2\right]$ **Reinforcement:** $f_{si} = E_{si}\varepsilon_{si} \le f_{yi}$ **Shear Stress on Crack:** $v_{ci} \le \frac{2.17\sqrt{f'_c}}{0.31 + \frac{24 w_m}{a + 0.63}}$ (psi, in.)	**Average Stresses:** $\sigma_x = f_{cx} + \rho_x f_{sx}$ $\sigma_y = f_{cy} + \rho_y f_{sy}$ $\tau_{xy} = v_{cxy}$ **Crack Stresses:** $f_{c1} = \sum \rho_i (f_{scri} - f_{si})\cos^2\theta_{ni}$ $v_{ci} = \sum \rho_i (f_{scri} - f_{si})\cos\theta_{ni}\sin\theta_{ni}$

Figure 4-3: Summary of MCFT Equations (adapted from Bentz et al., 2006)

4.1.3 Disturbed Region Analysis

Classical beam theory is based on the assumptions that i) plane sections remain plane, and ii) transverse stresses (i.e., clamping stresses) are negligible. A region of a member which complies with these assumptions is typically referred to a "beam region." Conversely, regions where support or heavily-concentrated loading causes beam response

to greatly deviate from these assumptions are called "disturbed regions" (Schlaich, Schafer and Jennewein, 1987). Simplified MCFT procedures (e.g., Bentz et al., 2006) that are formulated based on classical beam theory have been shown to be accurate, but are arguably not adequate for disturbed region analysis. This subsection will elaborate on concepts used to incorporate features permitting disturbed region analysis in the mechanics-based crack assessment procedure.

Deep beams are those with shear span-to-depth ratios (a/d) less than approximately 2 to 2.5. In beams with such relatively short shear spans, the flow of forces between the load and support gives rise to nonlinear shear strains which govern the beam's behavior (Birrcher et al., 2009). Given this nonlinear strain distribution, it is necessary to include disturbed region effects for the analysis of deep beams, that is, average y-direction stresses are nonzero. Generally, the analysis of disturbed regions requires alternative analysis methods that fall outside of sectional analysis and design procedures (e.g., nonlinear finite element analyses, strut-and-tie modeling). However, two research programs from the University of Toronto (Acevedo, 2008; Uzel, 2003) developed expressions to estimate the distribution of clamping stresses for incorporation within sectional design and analysis procedures (R2K and CSA Design Code). Using the nonlinear finite element analysis program TRIX97 (Vecchio, 1989), Uzel (2003) proposed a series of equations (Equation 4-8 through Equation 4-10) to determine a triangular (bilinear) clamping stress distribution at any given section in the shear span of a RC beam subjected to shear. Equation 4-8 determines the dispersion length (c) over which the load influences clamping stresses. The maximum value of clamping stress (σ_y) and location through the depth (h_y) are given by Equation 4-9 and Equation 4-10, respectively. The top and bottom face of the beam have clamping stress equal to zero to maintain equilibrium and the influence attributed to multiple concentrated loads within a span are accounted using superposition. Figure 4-4

shows assumed clamping stress distributions for the load and support point along the shear span (a) of a typical RC beam member. Results from both series of analytical programs showed an improvement in the performance of the sectional procedures that were enhanced with clamping stress effects. Therefore, it was sought to incorporate these effects similarly for the procedure being presented herein.

$$c = \left(1.5 - \frac{3}{4}\frac{l_b}{a}\right) h \qquad \textbf{Equation 4-8}$$

$$\sigma_y = \begin{cases} \frac{V}{ab}\left(\frac{2.5}{0.6+4\frac{L_s}{c}} - 0.5\right) & \text{if } L_s < c \\ 0 & \text{if } L_s \geq c \end{cases} \qquad \textbf{Equation 4-9}$$

$$h_y = h\left(1 - \frac{L_s}{c}\right) \qquad \textbf{Equation 4-10}$$

Where,
l_b = bearing plate length,
a = shear span,
h = total height of beam,
b = width of web,
V = shear in span caused by point load, and
L_s = location of interest.

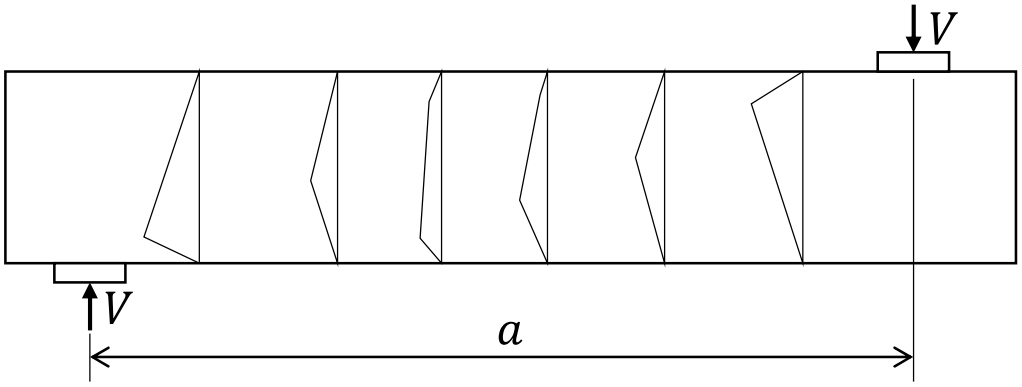

Figure 4-4: Assumed clamping stress distribution (adapted from Uzel, 2003)

In the mechanics-based crack assessment procedure presented in this thesis, the web is analyzed as an average, equivalent element resisting an average shear stress over the effective depth of the beam. In this context, an average (i.e., a constant through-depth)

clamping stress is used to incorporate disturbed region effects. To make use of the expressions presented by Uzel (2003), some changes were made to better suit the procedure at hand. First, like the approach of Acevedo (2008), the clamping stresses were normalized with respect to the shear stress because estimating 'unknown' shear stresses is one of the primary goals of the procedure. Converting the triangular distribution to an average and constant clamping stress over the beam depth (d_v) yields Equation 4-11, which is considered exclusively in the mechanics-based crack assessment procedure.

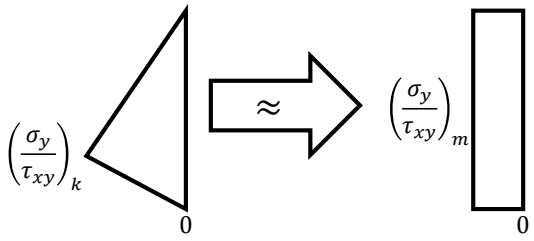

Figure 4-5: Clamping stress simplification

$$\frac{\sigma_y}{\tau_{xy}} = \begin{cases} \frac{1}{2}\frac{h}{a}\left(\frac{2.5}{0.6+4\frac{L_S}{c}} - 0.5\right) & \text{if } L_S < c \\ 0 & \text{if } L_s \geq c \end{cases} \qquad \textbf{Equation 4-11}$$

There are two important notes regarding the use Equation 4-11: 1) This expression cannot be used to incorporate the effects of distributed loads. Expressions exist that could be modified and implemented (Acevedo, 2008; Uzel, 2003), but have not been considered in this preliminary investigation. 2) The shear force must be relatively constant within the shear span, that is, it is assumed that the influence of self-weight effects is small relative to that of applied shear forces.

4.2 Preliminary Procedure

The previous section of this chapter summarized the foundation that forms the basis of the proposed mechanics-based crack assessment procedure. This section outlines the use of this foundation to assess in-service bridge members. Using data collected from a field

crack inspection, insights about the stress conditions of the beam web can be made. The two most important quantities are crack width and inclination. Although crack spacing is an important parameter, it can be estimated with expressions given in Section 4.1.1.

The first step of the procedure is to determine the average biaxial stress condition acting on the idealized RC element. Using Equation 4-2, an estimate can be made regarding the average principal tensile strain corresponding to the average visual cracking condition of the beam web. Next, Equation 4-11 is used to estimate the ratio of average y-direction normal stresses to average shear stresses acting on the idealized element. With these two items, an iterative solution procedure, as shown in Figure 4-6, can be used to solve for the final stress proportion (x-direction normal stress to shear stress). First, an initial guess for the principal compression strain is made. Next, by solving the system of equations given in Figure 4-3, loading proportions between normal (x- and y-direction) and shear stresses can be estimated. At this point, a check is made on the clamping (y-direction) stress proportions. If the results of the current iteration do not satisfy the proportion calculated at the beginning of the procedure then a new value of principal compression strain is selected and the loop is repeated. Once the estimated clamping stress-shear stress ratio is satisfied, the next portion of the procedure can begin.

The second portion of the procedure involves forecasting member response based on the estimated initial stress state. Two forecasting approaches were investigated: 1) free load proportion (i.e., using MCFT to update the stress state to maintain a fixed crack angle) and 2) fixed load proportion based on a fixed crack modeling procedure. The first approach can be envisioned as a direct continuation of the first portion of the procedure. Crack inclination remains fixed, while crack widths are incremented at each load stage. In this case, only clamping stress proportion is fixed and the x-direction stress proportion is left free to satisfy the no crack slip requirement in the MCFT based procedure. In the second

forecasting approach, the x-direction stress proportion established in the first portion of procedure is treated as a fixed proportion and x- and y-direction stresses are incremented in proportion to the shear stress at each load stage. In this case, a fixed angle crack procedure (with MCFT constitutive laws) is used to forecast failure. Once the failure state is reached, a global shear stress capacity check can be made. Using this value, it is possible to estimate the residual capacity of the in-service bridge member using Equation 4-12. After initial trial results were generated, the fixed proportion method was selected and used in the results presented in Section 4.3.

$$Residual\ capacity = \left(1 - \frac{V_a}{V_u}\right) \cdot 100\% \qquad \textbf{Equation 4-12}$$

Where,
V_a = applied shear force calculated in part 1 of the procedure,
V_u = failure shear force calculated in part 2 of the procedure.

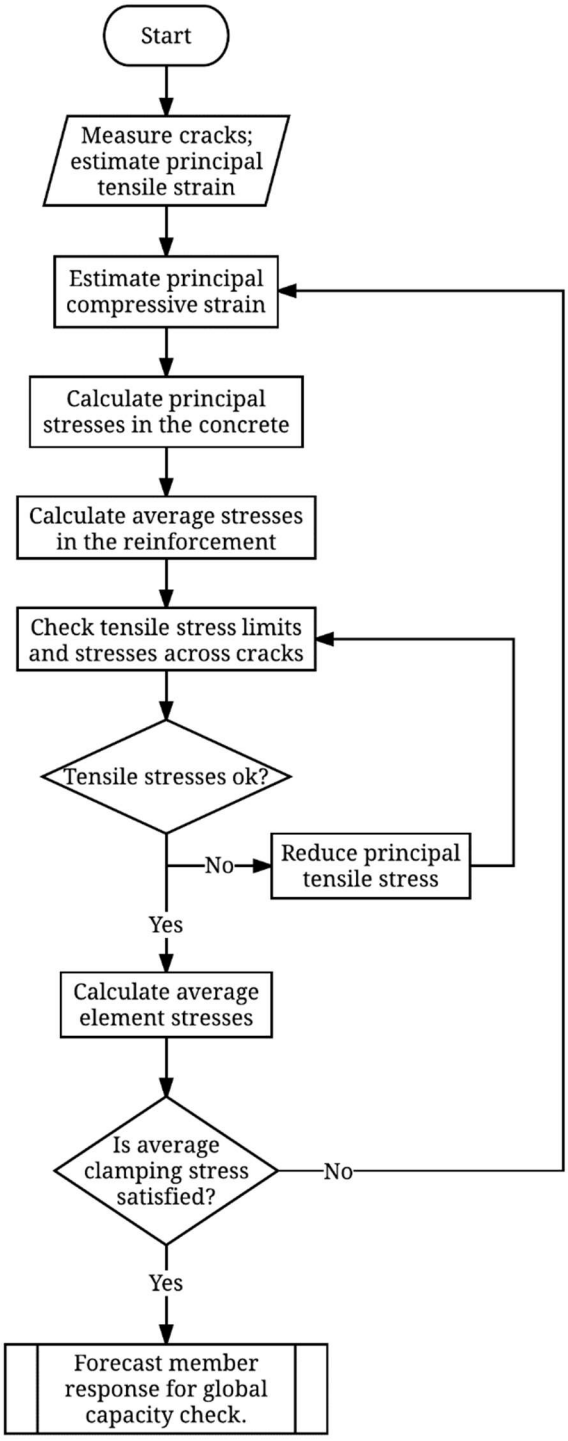

Figure 4-6: Procedure overview

4.3 PRELIMINARY PROCEDURE APPRAISAL

This section uses sources contained in the VCMD developed in Chapter 3 to assess the effectiveness of the mechanics-based crack assessment procedure presented in Section 4.2. 420 sets of crack widths and inclinations were used to assess the health of 74 damaged RC beams at various load levels. The beams analyzed came from three sources: Bracci et al. (2000), Birrcher et al. (2009), and Larson et al. (2013). All three projects focused on bent cap style members, that is, relatively large, deep beams with evenly distributed web reinforcement. Each project is briefly discussed and selected results are shown in sections 4.3.1 through 4.3.3.

4.3.1 Bracci et al. (2000)

Excessive cracking observed in in-service RC bent caps motivated TxDOT Research Project 0-1851 (Bracci et al., 2000). Sixteen full-scale bent caps with nominally identical geometries were constructed to observe the influence of a variety of reinforcement layouts on cracking behavior. Typical beam geometry is shown in Figure 4-7. Each beam was loaded monotonically to failure and crack widths were documented up to an applied load of approximately 360 kips, regardless of failure load. Crack patterns were photographed at most load levels, which were used as a means of estimating crack inclinations for the VCMD. A selection of relevant details are given in Table 4-1. More complete properties are in the VCMD or Bracci et al. (2000).

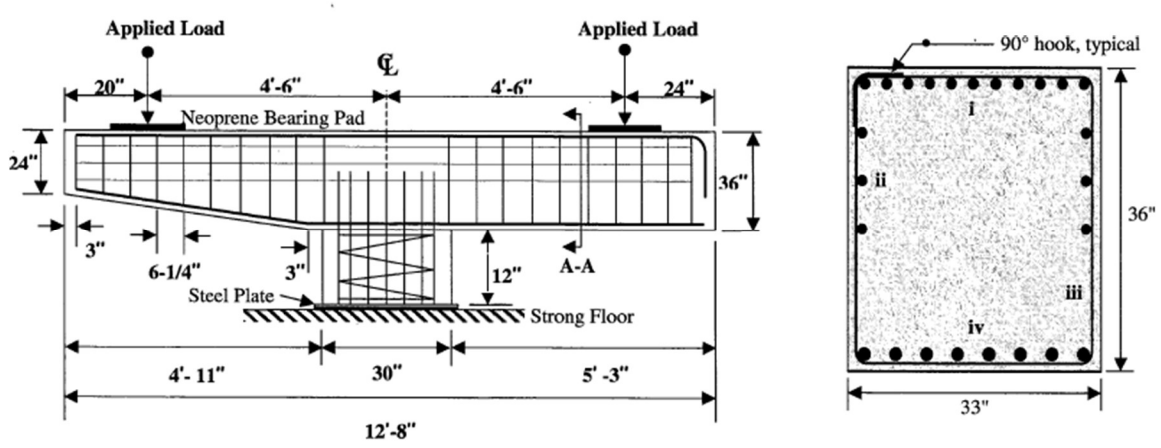

Figure 4-7: Beam geometry and cross-section (adapted from Bracci et al., 2000)

Table 4-1: Beam properties from Bracci et al. (2000)

Name	b_w (in.)	d (in.)	a/d	f'_c (psi)	ρ_l (%)	ρ_h (%)	ρ_v (%)
1A	33	32.9	1.64	6217	0.58	0.19	0.30
1B	33	32.9	1.64	5820	0.58	0.19	0.30
2A	33	32.9	1.64	6217	0.58	0.22	0.30
2B	33	32.9	1.64	5820	0.58	0.22	0.30
3C	33	32.9	1.64	6035	0.61	0.22	0.30
3D	33	32.9	1.64	5508	0.61	0.22	0.30
4C	33	32.7	1.65	6035	0.82	0.22	0.30
4E	33	32.7	1.65	7722	0.82	0.22	0.30
5D	33	32.9	1.64	5508	0.80	0.22	0.30
5E	33	32.9	1.64	7722	0.80	0.22	0.30
6F	33	32.7	1.65	5460	0.59	0.22	0.60
6G	33	32.7	1.65	5320	0.59	0.22	0.60
7F	33	32.9	1.64	5460	0.80	0.22	0.60
7H	33	32.9	1.64	5727	0.80	0.22	0.60
8G	33	32.9	1.64	5320	0.58	0.22	0.60
8H	33	32.9	1.64	5727	0.58	0.22	0.60

A total of 73 analyses were run for the beams comprising Table 4-1. Figure 4-8 shows the predicted-to-experimental comparisons for shear strength utilization (V_a/V_u), while Figure 4-9 shows residual capacity forecasts from six analyses. Note that the percentages being shown throughout the results section are complements of the residual capacity. The general trend is conservative, meaning the predicted load level is typically higher (i.e., closer to failure) than what was experimentally observed. The average predicted-to-experiment ratio for this dataset was 1.17 and the coefficient of variation (COV) was 20 %. Given the natural variability of concrete cracking behavior and the difficulties associated with accurately measuring and/or estimating cracking characteristics (e.g., widths, spacings, etc.), this conservativeness and level of variability seems within the bounds of reason. This suggests that at least as a reserve capacity estimate tool, the procedure presented in this chapter shows promise.

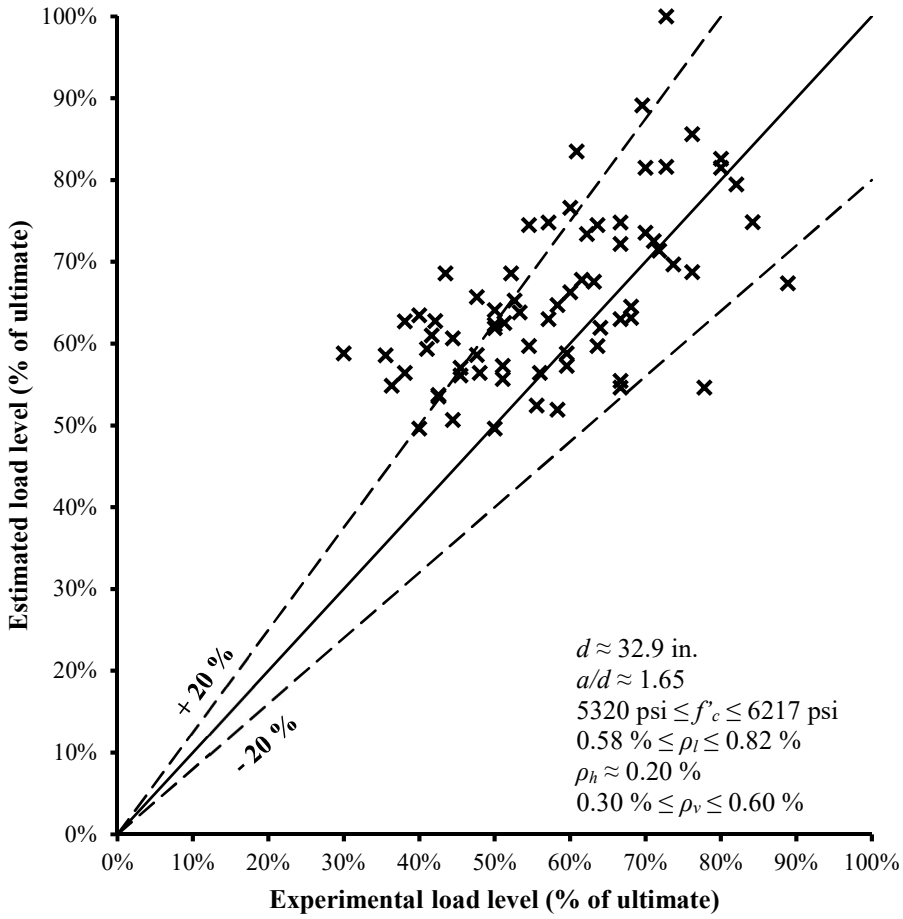

Figure 4-8: Results for beams tested by Bracci et al. (2000)

Input for the results shown in Figure 4-9 are based on crack conditions corresponding to service load level conditions, that is, approximately 40 to 60 % of ultimate capacity. The application of this procedure as a forecasting tool, that is, predicting future crack widths and their associated load levels is potentially unreliable based on some of these selected results. While many of the forecasts (1A, 2A, 3D, 7H, and 8H) capture future behavior reasonably well (within 20 % or so), others resulted in appreciable error (refer to beam 6G). Nevertheless, the results developed for the Bracci et al. testing program are very reasonable and support the general modeling procedure presented in this chapter.

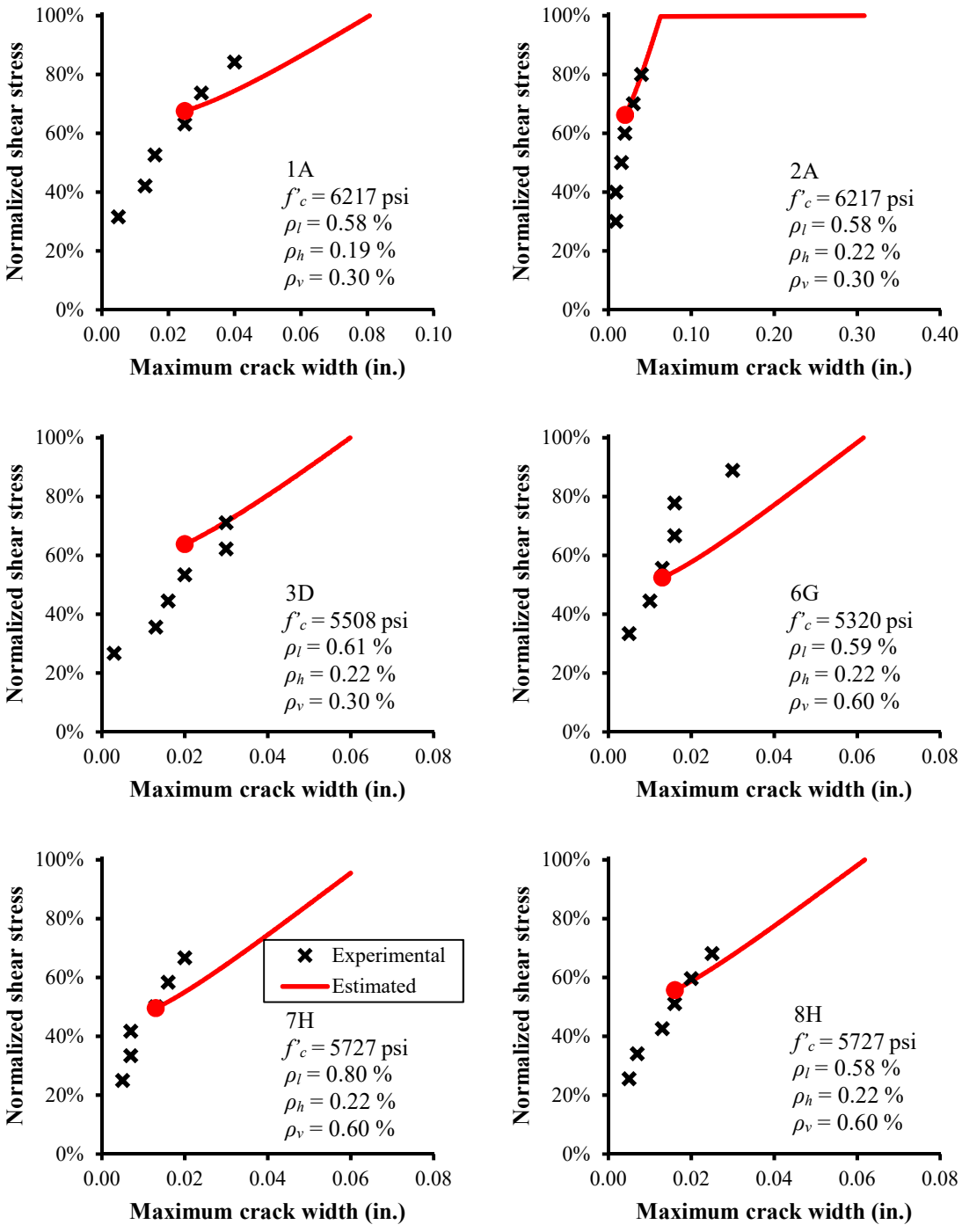

Figure 4-9: Selected forecasts for beams tested by Bracci et al. (2000)

4.3.2 Birrcher et al. (2009)

TxDOT Project 0-5253 (Birrcher et al., 2009) was an experimental study on strength and serviceability of RC deep beams. In this experimental program, 37 deep beam specimens with various geometries, web reinforcement details, and shear span-to-depth ratios were examined. The general test setup and sample member geometry is shown in Figure 4-10. Crack widths and patterns were documented over a wide variety of load stages. Of the 37 deep beams, 33 were used to assess the effectiveness of the mechanics-based crack assessment procedure presented in this chapter. Selected member properties are given in Table 4-2, with more complete properties being listed in Birrcher et al. (2009) or the VCMD.

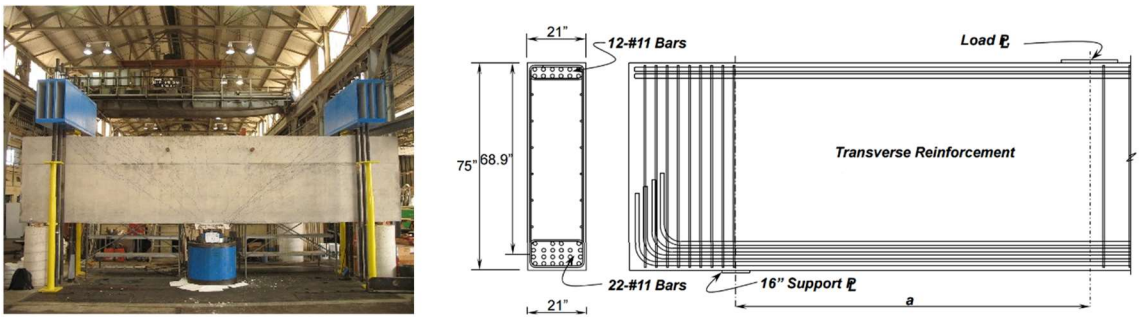

Figure 4-10: Experimental setup and beam geometry (adapted from Birrcher et al., 2009)

Table 4-2: Beam properties from Birrcher et al. (2009)

Name	b_w (in.)	d (in.)	a/d	f'_c (psi)	ρ_l (%)	ρ_h (%)	ρ_v (%)
I-03-2	21	38.5	1.84	5240	2.29	0.33	0.29
I-03-4	21	38.5	1.84	5330	2.29	0.33	0.30
I-02-2	21	38.5	1.84	3950	2.29	0.20	0.20
I-02-4	21	38.5	1.84	4160	2.29	0.20	0.21
II-03-CCC2021	21	38.6	1.84	3290	2.31	0.45	0.31
II-03-CCC1007	21	38.6	1.84	3480	2.31	0.45	0.31
II-02-CCC1007	21	38.6	1.84	3140	2.31	0.20	0.20
II-02-CCC1021	21	38.6	1.84	4620	2.31	0.19	0.20
II-03-CCT1021	21	38.6	1.84	4410	2.31	0.45	0.31
II-03-CCT0507	21	38.6	1.84	4210	2.31	0.45	0.31
II-02-CCT0507	21	38.6	1.84	3120	2.31	0.19	0.20
II-02-CCT0521	21	38.6	1.84	4740	2.31	0.19	0.20
III-1.85-00	21	38.6	1.84	3170	2.31	0.00	0.00
III-1.85-02	21	38.6	1.84	4100	2.31	0.19	0.20
III-1.85-025	21	38.6	1.84	4100	2.31	0.14	0.24
III-1.85-03	21	38.6	1.84	4990	2.31	0.29	0.29
III-1.85-01	21	38.6	1.84	5010	2.31	0.14	0.10
III-1.85-03b	21	38.6	1.84	3300	2.31	0.29	0.31
III-1.85-02b	21	38.6	1.84	3300	2.31	0.19	0.20
III-1.2-02	21	38.6	1.20	4100	2.31	0.19	0.20
III-1.2-03	21	38.6	1.20	4220	2.31	0.29	0.31
III-2.5-02	21	38.6	2.49	4630	2.31	0.19	0.20

Table 4-2 (cont.): Beam properties from Birrcher et al. (2009)

Name	b_w (in.)	d (in.)	a/d	f'_c (psi)	ρ_l (%)	ρ_h (%)	ρ_v (%)
III-2.5-03	21	38.6	2.49	5030	2.31	0.29	0.31
IV-2175-1.85-02	21	68.9	1.85	4930	2.37	0.19	0.21
IV-2175-1.85-03	21	68.9	1.85	4930	2.37	0.29	0.31
IV-2175-2.5-02	21	68.9	2.5	5010	2.37	0.21	0.21
IV-2175-1.2-02	21	68.9	1.2	5010	2.37	0.21	0.21
IV-2123-1.85-03	21	19.5	1.85	4160	2.32	0.30	0.30
IV-2123-1.85-02	21	19.5	1.85	4220	2.32	0.17	0.20
IV-2123-2.5-02	21	19.5	2.5	4570	2.32	0.17	0.20
M-03-4-CCC2436	36	40	1.85	4100	2.93	0.27	0.31
M-03-4-CCC0812	36	40	1.85	3000	2.93	0.27	0.31
M-02-4-CCC2436	36	40	1.85	2800	2.93	0.22	0.22

Diagonal cracking in deep beams is often characterized by primary shear cracks extending from the load to support point, as shown in Figure 4-11. For comparison purposes, two types of data have been separated. The black x's in Figure 4-12 represent data points where crack inclinations were reported or taken from available crack patterns. The red diamonds represent data points where crack inclination was estimated from geometry using Equation 4-13.

$$\theta_{cr} \approx \operatorname{atan}\frac{d}{a} \qquad \textbf{Equation 4-13}$$

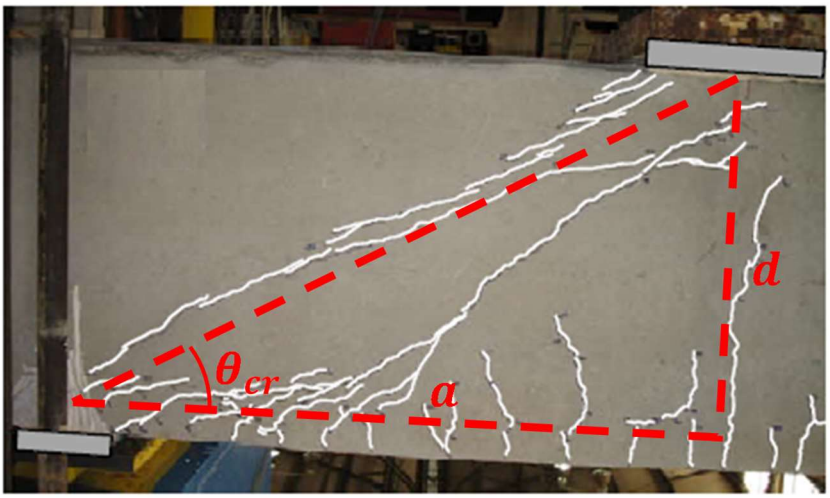

Figure 4-11: Approximation for crack inclination (adapted from Birrcher et al., 2009)

The trend in both sets is conservative, similarly to results from Section 4.3.1. For beams analyzed without Equation 4-13, the average predicted-to-experiment ratio is 1.43 and the COV is 56 %. Results from beams with inclinations from Equation 4-13 have an average predicted-to-experiment ratio of 1.48 with a COV of 45 %. The procedure fared relatively poorly in these analyses, particularly at lower load levels. It is possible there were other factors at play influencing the accuracy in addition to those which are inherent to the problem (cracking is unpredictable and measurements can be unreliable). Additional comments will be made in Section 4.4.

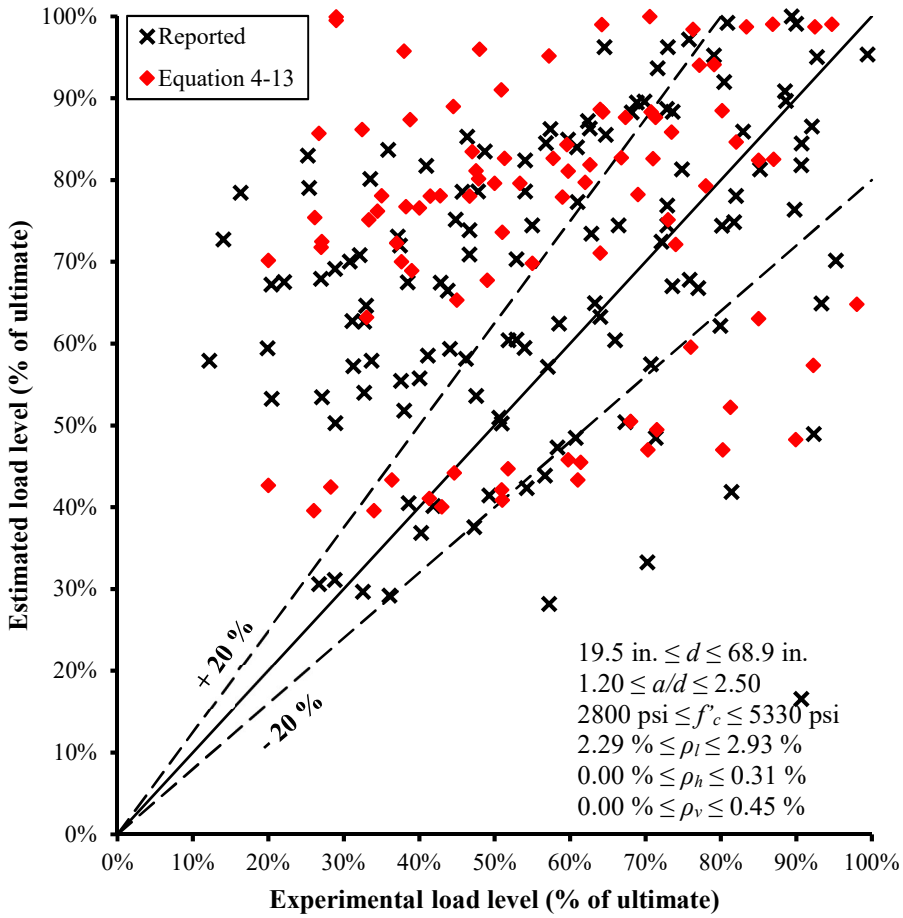

Figure 4-12: Results for beams tested by Birrcher et al. (2009)

Figure 4-13 again shows that the procedure can sometimes be an effective means of forecasting future behavior, while other times only providing a reasonable prediction of residual capacity. It is unsurprising, given the level of variation and overall performance for the beams analyzed in this series, that the behavioral forecasts sometimes show significant deviations from actual behavior. Note that the selected results all used inclinations either reported or taken from crack patterns.

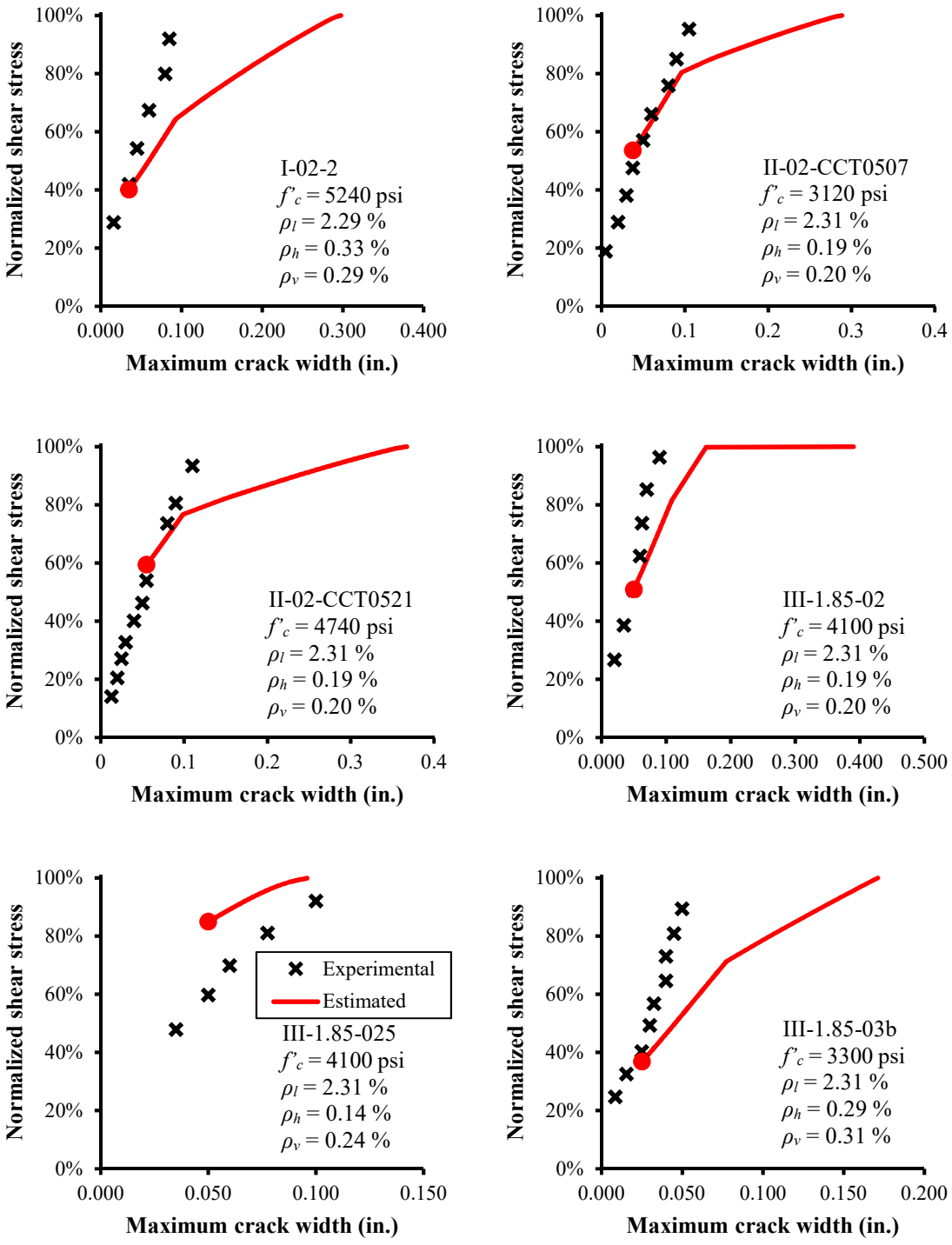

Figure 4-13: Selected forecasts for beams tested by Birrcher et al. (2009)

4.3.3 Larson et al. (2013)

The last set of beams analyzed in this thesis are inverted-T beams tested as part of TxDOT Project 0-6416 (Larson et al., 2013). In this program, 33 full scale RC inverted-T beams with variable ledge and web properties were tested. Tested properties include the following: ledge length, ledge depth, web reinforcement, loading scheme, and effective depth. Sample beam geometry is shown in Figure 4-14. Crack widths and patterns were documented over a large variety of load levels to empirically correlate maximum crack widths to load on the beam. Of the 33 beams, 25 were deemed suitable (i.e., shear-based failure, adequate crack documentation, etc.) to appraise the mechanics-based crack assessment procedure presented herein. A selection of relevant details are given in Table 4-3. More complete properties are in the VCMD or Larson et al. (2013).

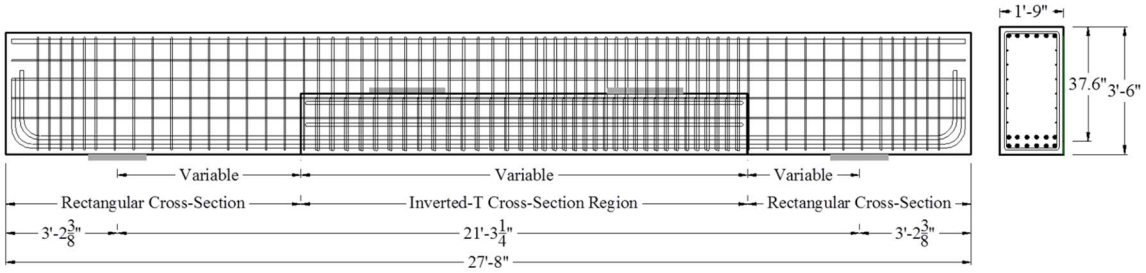

Figure 4-14: Beam geometry and cross-section (adapted from Larson et al., 2013)

Table 4-3: Beam properties from Larson et al. (2013)

Name	b_w (in.)	d (in.)	a/d	f'_c (psi)	ρ_l (%)	ρ_h (%)	ρ_v (%)
DC3-42-1.85-03	21	37.6	1.85	4568	2.37	0.30	0.30
DS3-42-1.85-03	21	37.6	1.85	4568	2.37	0.30	0.30
SC3-42-1.85-03	21	37.6	1.85	5873	2.37	0.30	0.30
SS3-42-1.85-03	21	37.6	1.85	5891	2.37	0.30	0.30
SL3-42-1.85-03	21	37.6	1.85	5037	2.37	0.30	0.30
SS1-75-1.85-03	21	68.2	1.87	3127	2.40	0.30	0.30
SS1-42-1.85-03	21	37.6	1.85	5258	2.37	0.30	0.30
DS1-42-1.85-03	21	37.6	2.50	5389	2.37	0.30	0.30
DS1-42-2.50-03	21	37.6	1.85	5024	2.37	0.60	0.60
DS1-42-1.85-06	21	37.6	2.50	5088	2.37	0.60	0.60
DS1-42-2.50-06	21	37.6	1.85	4830	2.37	0.60	0.60
DL1-42-1.85-06	21	37.6	2.50	4986	2.37	0.60	0.60
DL1-42-2.50-06	21	37.6	2.50	5891	2.37	0.30	0.30
SS3-42-2.50-03	21	37.6	2.50	5873	2.37	0.30	0.30
SC3-42-2.50-03	21	37.6	2.50	5687	2.37	0.30	0.30
DS3-42-2.50-03	21	37.6	1.85	4929	2.37	0.30	0.30
DL1-42-1.85-03	21	37.6	2.50	4929	2.37	0.30	0.30

Table 4-3 (cont.): Beam properties from Larson et al. (2013)

Name	b_w (in.)	d (in.)	a/d	f'_c (psi)	ρ_l (%)	ρ_h (%)	ρ_v (%)
DL1-42-2.50-03	21	37.6	1.85	5250	2.37	0.60	0.60
SL3-42-1.85-06	21	37.6	1.85	3727	2.37	0.60	0.60
DC1-42-1.85-06	21	37.6	2.50	5703	2.37	0.30	0.30
SS1-42-2.50-03	21	37.6	1.85	5721	2.37	0.30	0.30
SL1-42-2.50-03	21	37.6	2.5	4281	2.37	0.30	0.30
DS1-42-1.85-06/03	21	37.6	1.85	4173	2.37	0.30	0.60
DS1-42-2.50-06/03	21	37.6	2.50	4173	2.37	0.30	0.60
DC1-42-1.85-03	21	37.6	1.85	4303	2.37	0.30	0.30

As was the case for the beams tested by Birrcher et al. (2009), analyses were performed using crack inclinations that were either reported or were estimated on the basis of documented crack patterns (black x's on Figure 4-15, 39 total) while others used approximate crack inclinations (red diamonds on Figure 4-15, 91 total) estimated with Equation 4-13. The 39 analyses with reported or estimated crack inclinations had an average predicted-to-experiment ratio of 0.98 with a COV of 22 %. These results are more consistent with those presented in Section 4.3.1, that is, good predicted-to-experiment ratios and a reasonable level of variation. However, note that in this case the conservativeness observed in the first two analysis series is absent. The 91 analyses with approximate crack inclinations had an average ratio of 1.42 and COV of 33 %. Again, note that approximate crack inclinations trend conservatively and with a high COV, particularly at low load levels.

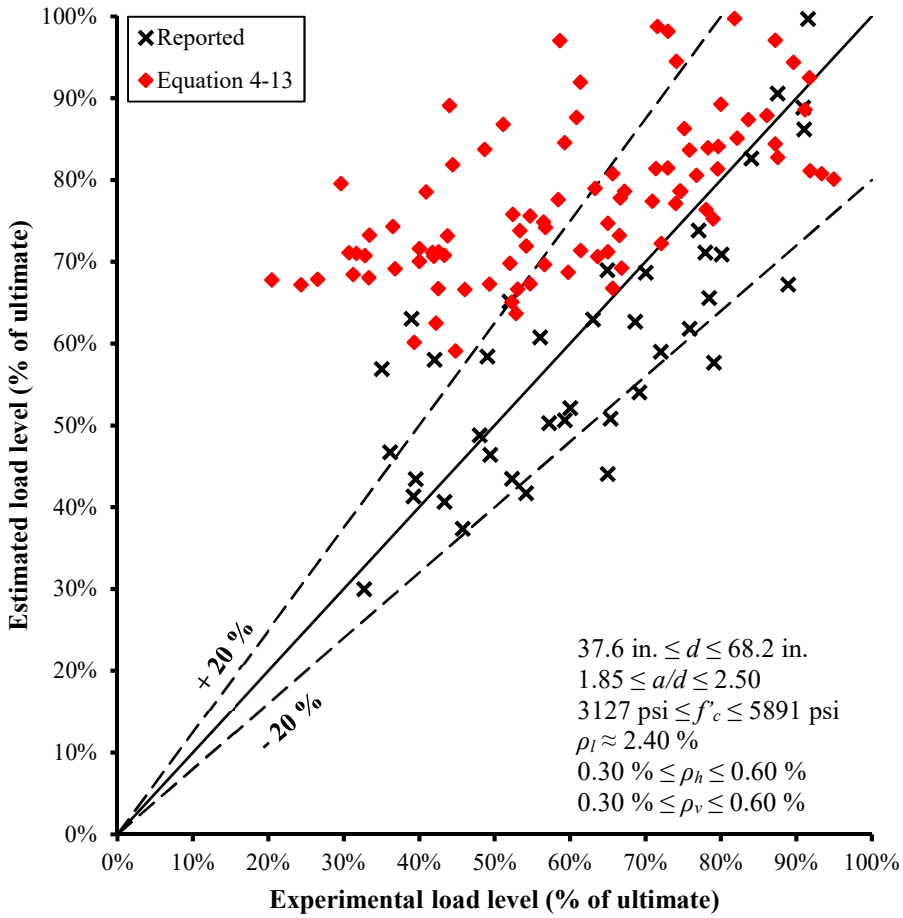

Figure 4-15: Results for beams tested by Larson et al. (2013)

Figure 4-16 shows six sample forecasts for beams from Larson et al. (2013). Accuracy in predicting future crack widths and their associated load levels are in line with results already presented in Figure 4-9 and Figure 4-13; in some cases, a very good fit is achieved while other cases illustrate appreciable error. Overall, the results in this section show promise for the mechanics-based crack procedure presented in this chapter, particularly as a residual capacity prediction tool.

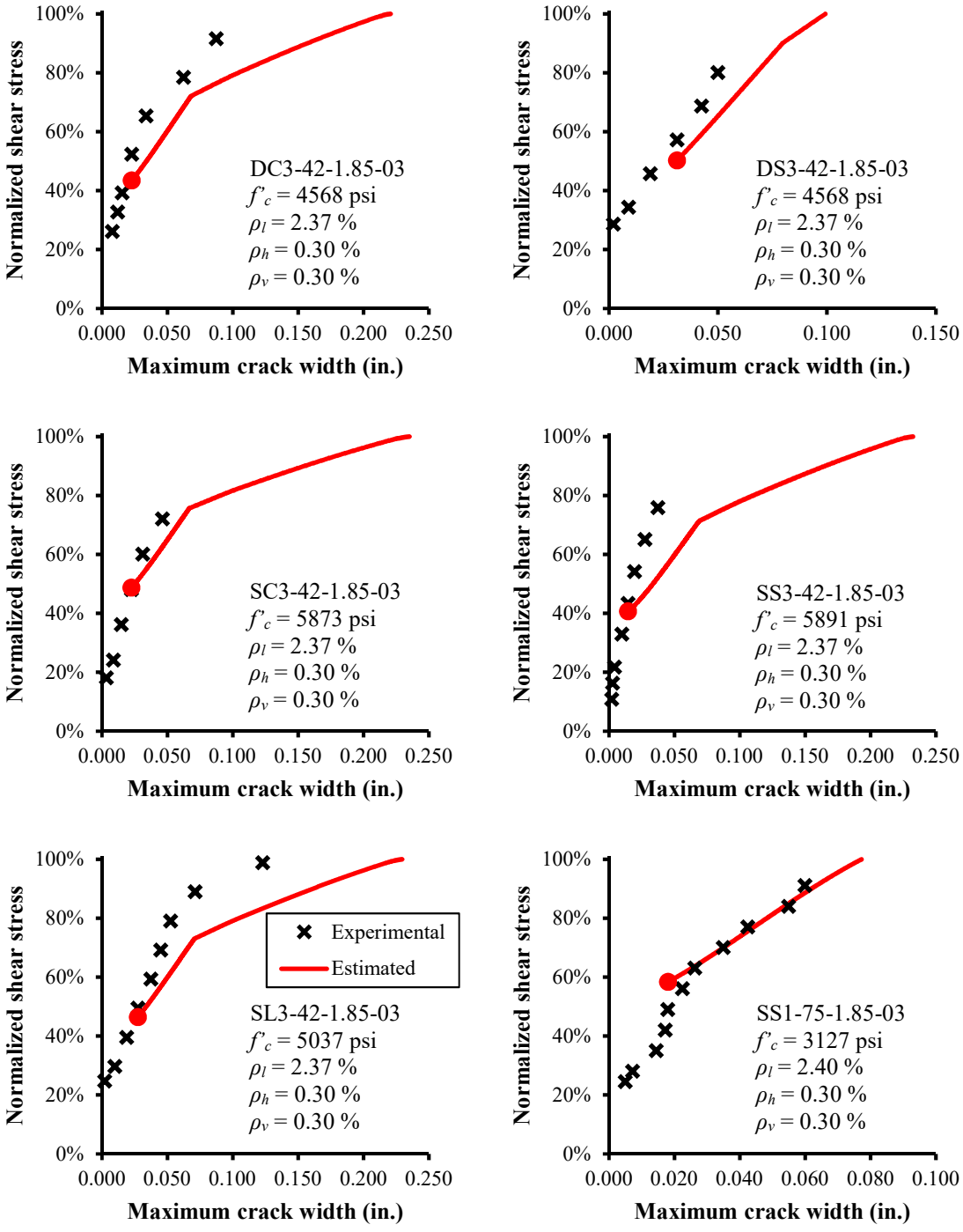

Figure 4-16: Selected forecasts for beams tested by Larson et al. (2013)

4.4 DISCUSSION

This chapter presented and appraised a methodology for the assessment of cracked RC deep beams using visually observed crack measurements as the primary basis of assessment. The backbone of the proposed procedure relies on an inverse-solution of the MCFT (Vecchio and Collins, 1986) approach, in addition to supplementary models (CEB-FIP, 1978; Uzel, 2003). Using this procedure, a normalized load level estimate (V_a/V_u) is generated, from which an estimation about the structure's health and residual capacity can be made.

Of importance to the procedure is how crack spacing and width models are used. Several different models have been proposed in the past half-century and all account for key variables (reinforcement layout, size, bond effects, etc.) slightly differently. Additionally, assumed variation between mean and maximum crack widths can influence results. This relationship has been shown to vary significantly based on several different experimental programs (Chowdhurry and Loo, 2001).

Many assessment procedures in the literature are either empirically derived, require complex FEA, or are limited to slender beams ($a/d \geq 3.0$) with known load ratios between shear and the two normal directions. The implementation of disturbed region analysis in a mechanics-based approach allows for more generality and can address a wider variety of analyses. In this procedure, triangular stress distributions formulated by Uzel (2003) were converted to equivalent rectangular stress distributions to account for disturbed region effects.

The procedure was appraised using three different experimental datasets (Birrcher et al., 2009; Bracci et al., 2000; Larson et al., 2013). Results varied substantially between the three datasets, shown all together in Figure 4-17. For results generated with known crack inclinations, the average predicted-to-experiment ratio was 1.28 and the COV was

49 %. For those results with crack inclinations approximated with Equation 4-13, the average ratio was 1.48 and the COV was 40 %. Note that, in the comparisons made in this chapter only normalized load levels were compared. Estimated shear stresses tended to vary from experimental results and were generally less reliable than the normalized values. The procedure presented by Calvi (2015) showed much better correlation for estimated shear stresses, but generally required known load levels, beam action, and crack slip measurements. It is believed that relaxing these requirements likely led to the unreliability of the shear stress magnitudes. Overall, results trended conservatively particularly at low load levels. This excessive conservativeness at low load levels is consistent with results for beams analyzed by Calvi (2015) and is potentially an inherent weakness in crack-based assessment procedures which utilize mechanics-based formulations.

As previously stated, the geometric approximation for crack inclination generally increased conservativeness and variability in the analysis results which suggests, as expected, that real, measured crack inclinations offer superior performance in this preliminary procedure. However, this does not resolve all the scatter in the results. A majority of the variability shown in Figure 4-17 occurred in the series of beams tested by Birrcher et al. (2009). There were several parameters varied in the beams tested by Birrcher et al. (2009) including the following: stirrup distribution, triaxial confinement (by way of bearing plate size), minimum web reinforcement, and member effective depth. Of these, the triaxially confined node region series consistently posed the most problems for the procedure. Nodal region (i.e., above or below load plates) influence on failure mode is not considered in this preliminary, beam web-based procedure; as such, the procedure will likely misrepresent beams which have strong influence from or fail inside a nodal region (i.e., outside the beam web). Other issues encountered in the procedure for this analysis

series were beams with little-to-no web reinforcement from the minimum web reinforcement series, which is another potential deficiency in the procedure.

Despite some shortcomings in crack-based predictions for beams tested by Birrcher et al. (2009), results from beams tested by Bracci et al. (2000) and Larson et al. (2013) show satisfactory performance. This approach is reasonably simple and utilizes simple details regarding concrete and reinforcement geometries and properties. Additionally, it is implementable in basic spreadsheet-type programs or other software where iterative/goal-seeking solution procedures can be used.

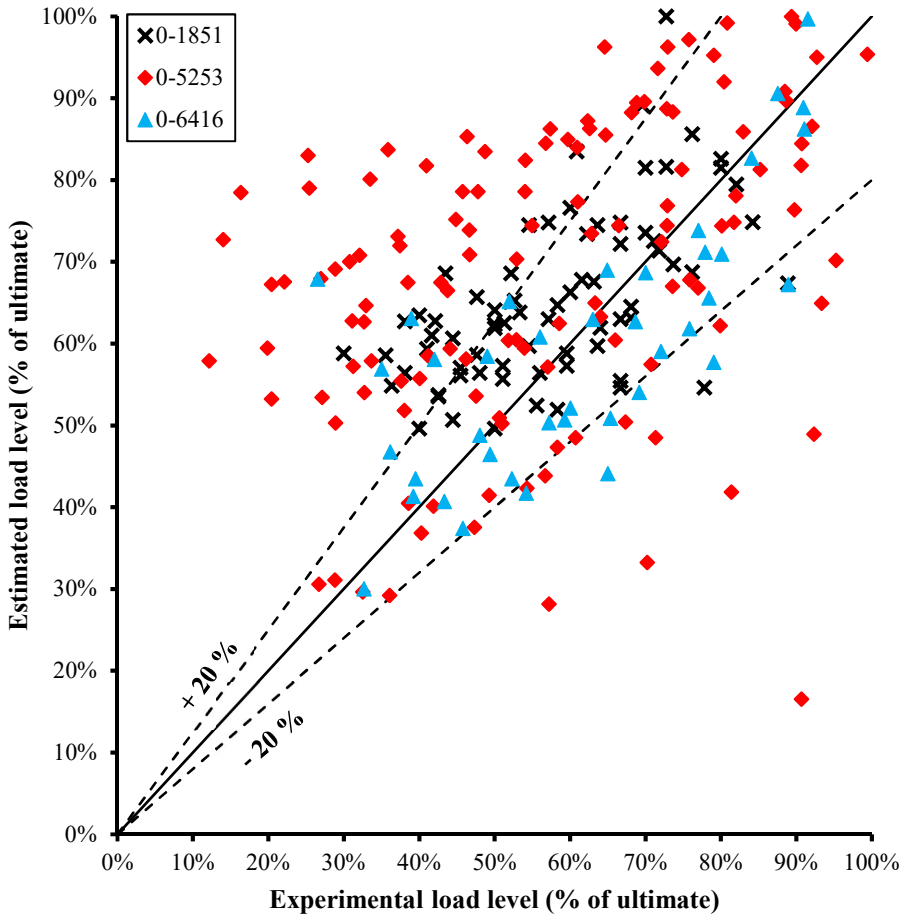

Figure 4-17: All results (Birrcher et al., 2009; Bracci et al., 2000; Larson et al., 2013)

Chapter 5: Conclusions and Recommendations

As the inventory of aging RC infrastructure continues to deteriorate, the methods that engineers and inspectors use to monitor and assess in-service structures must also mature. To this end, a preliminary mechanics-based procedure was proposed to assess damaged RC elements based on visually observed cracks. The mechanics-based procedure used the MCFT (Vecchio and Collins, 1986) as its core and was combined with supplementary models (CEB-FIP, 1978; Uzel, 2003) to provide residual capacity estimates for cracked RC elements. Procedure appraisal was completed using three experimental series (Birrcher et al., 2009; Bracci et al., 2000; Larson et al., 2013), all of which focused on relatively large, deep beams. This type of member was identified in field data review in Chapter 1 as one being prone to few moderate-to-severe cracks, which is not always easily assessed by the qualitative tools employed in practice. The procedure showed promise as a means of estimating residual capacity and giving insight into future structural behavior.

5.1 CONCLUSIONS

Based on the analytical study presented herein, the following conclusions can be made:

- **Not all cracks are equivalent.** Based on a review of 155 different RC elements with a variety of construction details, parameters such as size effect and reinforcement detailing play a significant role in crack behavior and should be accounted for in damage-based assessment procedures.
- **Crack width is not sensitive to shear span-to-depth ratio.** Based on a review of the VCMD and conclusions made by past research programs at the University of Texas at Austin (Birrcher et al., 2009; Larson et al., 2013), there are no clear trends between crack width and shear span-to-depth ratio.

- **Visually observed crack characteristics can be linked to residual capacity of cracked RC.** Results from the present study, and results presented by others (e.g., Calvi, 2015), show that using visually observed crack measurements can provide reasonable residual capacity estimates for a variety of different RC elements and loading conditions. Furthermore, the results developed using the preliminary assessment approach were generally found to trend conservatively, which is important in the context of public safety when assessing in-service structures. The procedure's performance varied, but showed promise. See Section 5.2 for recommendations on how to improve the procedure.
- **In RC elements with large amounts of reserve capacity, mechanics-based procedures which use a single, equivalent beam web element tend to be overly-conservative.** In both results from the present study and Calvi (2015), assessments done at low load levels tended to predict significantly less reserve capacity than what was available. However, at low load levels and with only limited concrete cracking, it is likely that traditional visual inspection procedures would deem further analyses unnecessary.
- **This preliminary procedure is not adequate for addressing failures that take place outside of uniform stress fields or in elements with factors that exacerbate nonuniform stress fields.** Analyses on beams tested by Birrcher et al. (2009) demonstrated some inadequacies in the proposed preliminary procedure. These discrepancies in accuracy are likely related to factors that give rise to nonuniform stress distributions (e.g., triaxially confined nodes, light web reinforcement, etc.). To truly capture nonuniform stress distributions, it is typically necessary to use a higher number of

smaller elements (like mesh refinement in FEA). In this light, it makes sense that a single element approach would encounter difficulties in these more complicated analysis cases. However, in cases where reasonably uniform stress fields are present, this procedure is a relatively simple and rational tool for assessing in-service structures.

5.2 RECOMMENDATIONS FOR FUTURE WORK

This thesis represents what is a largely ongoing process in the field of assessing cracked RC elements. Many of the procedures that have been presented in the literature require additional development or experimental verification. As such, the following recommendations are made for further exploration:

- **Existing damage assessment procedures for cracked RC require more rigorous experimental verification.** Nearly all the procedures in the literature would benefit from additional verification, especially where none has been done. The VCMD is a reasonable tool for accomplishing this goal and has been shown to be useful in assessing the mechanics-based procedure presented in this thesis.
- **More experimental work with extensive crack measurement tracking should be completed.** In much of the literature, crack information is reported at only a few load levels and the information provided is relatively limited (e.g., only maximum crack widths near ultimate). To facilitate more effective crack-based assessment procedures, more crack characteristics (including crack width, inclination, spacing, and slip) should be monitored and reported.

- **Switching from the rotating-crack MCFT-base to a hybrid rotating-/fixed-crack base model (e.g., Disturbed Stress Field Model).** The inclusion of crack slip input seemingly improved accuracy in the work completed by Calvi (2015); as such, it may be prudent to include in future mechanics-based procedures. However, slip is often difficult to measure even in a controlled laboratory environment, let alone an in-service structure, and should be included in a way which does not overly complicate the inspection/measurement process.
- **Time-based effects should be studied and potentially included in future analysis procedures.** To date, a majority of the experimentally validated procedures were done with elements that were tested relatively soon after casting and had relatively short-term loading procedures. In real structures, concrete will have time to age and may have strengths higher than the design-specified values. This could be addressed using a tiered analysis process where cores are taken to verify in-situ concrete strengths if a preliminary analysis with design values failed. Also, real structures are never subjected to the highly-idealized loading protocols (e.g., monotonic, cyclic, or reverse-cyclic) or the idealized loading proportions that are employed in the laboratory setting. As such, damage patterns in real structures may not be accurately replicated in testing programs. Furthermore, in decades-old structures, time-based effects such as creep will inevitably play a role in the crack widths which are monitored. To provide as realistic assessment procedure as possible, the influence of these factors on crack behavior over a structure's service life should be studied and potentially included in future damage assessment procedures.

- **Additional work should be done to incorporate the influence of nodal region influence, light web reinforcement, etc.** Beam analyses from Bracci et al. (2000) and Larson et al. (2013) fared relatively well, while those from Birrcher et al. (2009) generally did not. There were a few key variables (e.g., triaxial confinement) which seem responsible for the procedure's inability to adequately capture behavior. Supplementary factors or checks should be investigated and incorporated to address these weaknesses in the procedure. It is imperative that as many failure modes as possible be included in the procedure to increase the reliability for assessing in-service structures.

Appendix A: Visual Crack Measurement Database

The VCMD is available in PDF form as the supplementary file "VCMD." It includes a sample report, member properties, and crack data for 155 RC members at load levels ranging from 10 % to approximately 100 % of ultimate. Refer to Chapter 3 for additional information regarding what information is included in the member properties and crack data section.

Appendix B: Preliminary Procedure Appraisal Results

Results from the analyses are shown graphically in Chapter 4. This appendix contains crack widths and inclinations used in the analyses, as well as the estimated load levels shown in plots within Section 4.3 and 4.4.

Table B-1: Results from beams tested by Bracci et al. (2000)

Member Name	V_a/V_u (exp)	w_k (in.)	θ_{cr} (deg)	V_a/V_u (est)	est/ exp
1A	42%	0.013	47.°	63%	1.49
1A	53%	0.016	39.°	65%	1.24
1A	63%	0.025	39.°	68%	1.07
1A	74%	0.030	39.°	70%	0.95
1A	84%	0.040	39.°	75%	0.89
1B	30%	0.010	60.°	59%	1.96
1B	40%	0.013	60.°	63%	1.59
1B	50%	0.016	52.°	62%	1.24
1B	60%	0.035	52.°	77%	1.28
1B	70%	0.040	52.°	81%	1.16
1B	80%	0.040	52.°	81%	1.02
2A	50%	0.016	48.°	64%	1.28
2A	60%	0.020	48.°	66%	1.10
2A	70%	0.030	48.°	74%	1.05
2A	80%	0.040	48.°	83%	1.03
2B	41%	0.010	53.°	59%	1.45
2B	51%	0.016	46.°	63%	1.22
2B	62%	0.025	46.°	68%	1.10
2B	72%	0.030	46.°	71%	0.99
2B	82%	0.040	46.°	79%	0.97

Table B-1 (cont.): Results from beams tested by Bracci et al. (2000

Member Name	V_a/V_u (exp)	w_k (in.)	θ_{cr} (deg)	V_a/V_u (est)	est/ exp
3C	38%	0.013	59.°	63%	1.65
3C	48%	0.020	52.°	66%	1.38
3C	57%	0.030	52.°	75%	1.31
3C	67%	0.030	52.°	75%	1.12
3C	76%	0.040	52.°	86%	1.12
3D	36%	0.013	52.°	59%	1.65
3D	44%	0.016	52.°	61%	1.36
3D	53%	0.020	52.°	64%	1.20
3D	62%	0.030	52.°	73%	1.18
3D	71%	0.030	51.°	73%	1.02
4C	45%	0.016	54.°	57%	1.26
4C	55%	0.030	54.°	74%	1.37
4C	64%	0.030	54.°	74%	1.17
4C	73%	0.050	54.°	100%	1.38
4E	43%	0.016	57.°	69%	1.58
4E	52%	0.016	57.°	69%	1.31
4E	61%	0.025	57.°	83%	1.37
4E	70%	0.030	57.°	89%	1.28
5D	43%	0.013	45.°	54%	1.26
5D	51%	0.020	45.°	57%	1.12
5D	60%	0.020	45.°	57%	0.96
5D	68%	0.030	45.°	65%	0.95
5E	42%	0.013	47.°	61%	1.46
5E	50%	0.016	47.°	62%	1.25

Table B-1 (cont.): Results from beams tested by Bracci et al. (2000

Member Name	V_a/V_u (exp)	w_k (in.)	θ_{cr} (deg)	V_a/V_u (est)	est/ exp
5E	58%	0.020	47.°	65%	1.11
5E	67%	0.030	47.°	72%	1.08
6F	38%	0.013	56.°	56%	1.48
6F	48%	0.016	54.°	59%	1.23
6F	57%	0.020	54.°	63%	1.10
6F	67%	0.020	54.°	63%	0.94
6F	76%	0.025	54.°	69%	0.90
6G	44%	0.010	45.°	51%	1.14
6G	56%	0.013	45.°	52%	0.94
6G	67%	0.016	45.°	55%	0.82
6G	78%	0.016	45.°	55%	0.70
6G	89%	0.030	45.°	67%	0.76
7F	40%	0.013	49.°	50%	1.24
7F	48%	0.020	49.°	56%	1.18
7F	56%	0.020	49.°	56%	1.01
7F	64%	0.025	49.°	62%	0.97
7H	50%	0.013	45.°	50%	0.99
7H	58%	0.016	45.°	52%	0.89
7H	67%	0.020	45.°	55%	0.83
8G	36%	0.013	53.°	55%	1.51
8G	45%	0.016	49.°	56%	1.23
8G	55%	0.020	49.°	60%	1.09
8G	64%	0.020	49.°	60%	0.94
8G	73%	0.040	49.°	82%	1.12

Table B-1 (cont.): Results from beams tested by Bracci et al. (2000

Member Name	V_a/V_u (exp)	w_k (in.)	θ_{cr} (deg)	V_a/V_u (est)	est/ exp
8H	43%	0.013	43.°	54%	1.26
8H	51%	0.016	43.°	56%	1.09
8H	60%	0.020	43.°	59%	0.99
8H	68%	0.025	43.°	63%	0.93
				μ	**1.17**
				COV	**20 %**

Table B-2: Results from beams tested by Birrcher et al. (2009)

Member Name	V_a/V_u (exp)	w_k (in.)	θ_{cr} (deg)	V_a/V_u (est)	est/ exp
I-03-2	33%	0.013	30.°	65%	1.96
I-03-2	43%	0.020	30.°	67%	1.57
I-03-2	53%	0.025	30.°	70%	1.33
I-03-2	63%	0.030	30.°	73%	1.17
I-03-2	73%	0.035	30.°	77%	1.05
I-03-2	83%	0.048	30.°	86%	1.04
I-03-2	93%	0.060	30.°	95%	1.02
I-03-4	20%	0.012	28.°	67%	3.29
I-03-4	29%	0.016	28.°	69%	2.40
I-03-4	37%	0.023	28.°	73%	1.97
I-03-4	46%	0.030	28.°	79%	1.72
I-03-4	54%	0.035	28.°	82%	1.52
I-03-4	63%	0.040	28.°	86%	1.38
I-03-4	72%	0.050	28.°	94%	1.31
I-03-4	88%	0.080	28.°	91%	1.03
I-02-2	29%	0.016	60.°	31%	1.08
I-02-2	42%	0.035	40.°	40%	0.96
I-02-2	54%	0.045	40.°	42%	0.78
I-02-2	67%	0.060	40.°	50%	0.75
I-02-2	80%	0.080	40.°	62%	0.78
I-02-4	25%	0.018	26.°	83%	3.29
I-02-4	36%	0.023	26.°	84%	2.33
I-02-4	46%	0.028	26.°	85%	1.84
I-02-4	57%	0.030	26.°	86%	1.50

Table B-2 (cont.): Results from beams tested by Birrcher et al. (2009

Member Name	V_a/V_u (exp)	w_k (in.)	θ_{cr} (deg)	V_a/V_u (est)	est/ exp
I-02-4	68%	0.035	26.°	88%	1.30
I-02-4	79%	0.050	26.°	95%	1.20
I-02-4	90%	0.060	26.°	99%	1.10
II-03-CCC2021	31%	0.012	31.°	57%	1.83
II-03-CCC2021	41%	0.015	31.°	59%	1.42
II-03-CCC2021	52%	0.018	31.°	60%	1.17
II-03-CCC2021	64%	0.023	31.°	63%	0.99
II-03-CCC2021	77%	0.028	31.°	67%	0.87
II-03-CCC2021	91%	0.050	31.°	84%	0.93
II-03-CCC1007	34%	0.013	31.°	58%	1.72
II-03-CCC1007	44%	0.016	31.°	59%	1.35
II-03-CCC1007	53%	0.018	31.°	60%	1.14
II-03-CCC1007	63%	0.025	31.°	65%	1.03
II-03-CCC1007	72%	0.035	31.°	72%	1.00
II-03-CCC1007	80%	0.038	31.°	74%	0.93
II-03-CCC1007	90%	0.040	31.°	76%	0.85
II-02-CCC1007	57%	0.015	45.°	28%	0.49
II-02-CCC1007	70%	0.028	45.°	33%	0.47
II-02-CCC1007	81%	0.040	45.°	42%	0.51
II-02-CCC1007	92%	0.050	45.°	49%	0.53
II-02-CCC1021	36%	0.016	44.°	29%	0.81
II-02-CCC1021	47%	0.030	44.°	38%	0.79
II-02-CCC1021	58%	0.045	44.°	47%	0.81
II-02-CCC1021	71%	0.060	44.°	57%	0.81

Table B-2 (cont.): Results from beams tested by Birrcher et al. (2009

Member Name	V_a/V_u (exp)	w_k (in.)	θ_{cr} (deg)	V_a/V_u (est)	est/ exp
II-02-CCC1021	82%	0.085	44.°	75%	0.92
II-03-CCT1021	12%	0.012	31.°	58%	4.76
II-03-CCT1021	20%	0.016	31.°	59%	2.99
II-03-CCT1021	31%	0.023	31.°	63%	2.02
II-03-CCT1021	38%	0.030	31.°	67%	1.75
II-03-CCT1021	47%	0.035	31.°	71%	1.52
II-03-CCT1021	55%	0.040	31.°	74%	1.35
II-03-CCT1021	66%	0.040	31.°	74%	1.12
II-03-CCT1021	73%	0.040	31.°	74%	1.02
II-03-CCT1021	82%	0.045	31.°	78%	0.95
II-03-CCT1021	91%	0.050	31.°	82%	0.90
II-03-CCT1021	99%	0.070	31.°	95%	0.96
II-03-CCT0507	22%	0.013	27.°	68%	3.06
II-03-CCT0507	31%	0.019	27.°	70%	2.28
II-03-CCT0507	37%	0.023	27.°	72%	1.92
II-03-CCT0507	45%	0.028	27.°	75%	1.68
II-03-CCT0507	54%	0.033	27.°	79%	1.45
II-03-CCT0507	61%	0.040	27.°	84%	1.38
II-03-CCT0507	69%	0.048	27.°	89%	1.30
II-03-CCT0507	76%	0.060	27.°	97%	1.28
II-02-CCT0507	29%	0.020	36.°	50%	1.74
II-02-CCT0507	38%	0.030	36.°	52%	1.36
II-02-CCT0507	48%	0.038	36.°	54%	1.13
II-02-CCT0507	57%	0.050	36.°	57%	1.00

Table B-2 (cont.): Results from beams tested by Birrcher et al. (2009

Member Name	V_a/V_u (exp)	w_k (in.)	θ_{cr} (deg)	V_a/V_u (est)	est/ exp
II-02-CCT0507	66%	0.060	36.°	60%	0.92
II-02-CCT0507	76%	0.081	36.°	68%	0.89
II-02-CCT0507	95%	0.105	36.°	70%	0.74
II-02-CCT0521	14%	0.013	33.°	73%	5.19
II-02-CCT0521	20%	0.020	33.°	53%	2.61
II-02-CCT0521	27%	0.025	33.°	53%	1.97
II-02-CCT0521	33%	0.030	33.°	54%	1.65
II-02-CCT0521	40%	0.040	33.°	56%	1.39
II-02-CCT0521	46%	0.050	33.°	58%	1.26
II-02-CCT0521	54%	0.055	33.°	59%	1.10
II-02-CCT0521	74%	0.080	33.°	67%	0.91
II-02-CCT0521	93%	0.110	33.°	65%	0.70
III-1.85-00	27%	0.030	37.°	68%	2.52
III-1.85-00	33%	0.038	37.°	63%	1.92
III-1.85-00	38%	0.050	37.°	55%	1.48
III-1.85-00	51%	0.063	37.°	50%	0.99
III-1.85-00	61%	0.094	37.°	48%	0.80
III-1.85-00	71%	0.100	37.°	48%	0.68
III-1.85-00	91%	0.160	24.°	17%	0.18
III-1.85-02	27%	0.020	45.°	31%	1.15
III-1.85-02	39%	0.035	45.°	40%	1.05
III-1.85-02	51%	0.050	45.°	51%	1.01
III-1.85-02	62%	0.060	26.°	87%	1.40
III-1.85-02	74%	0.063	26.°	88%	1.20

Table B-2 (cont.): Results from beams tested by Birrcher et al. (2009

Member Name	V_a/V_u (exp)	w_k (in.)	θ_{cr} (deg)	V_a/V_u (est)	est/ exp
III-1.85-02	85%	0.070	26.°	81%	0.95
III-1.85-025	48%	0.035	26.°	79%	1.64
III-1.85-025	60%	0.050	26.°	85%	1.42
III-1.85-025	70%	0.060	26.°	90%	1.28
III-1.85-025	92%	0.100	26.°	87%	0.94
III-1.85-03	32%	0.013	26.°	71%	2.21
III-1.85-03	47%	0.025	26.°	74%	1.58
III-1.85-03	61%	0.033	26.°	77%	1.27
III-1.85-03	75%	0.040	26.°	81%	1.09
III-1.85-03	89%	0.055	26.°	90%	1.01
III-1.85-01	44%	0.017	26.°	66%	1.52
III-1.85-01	59%	0.038	26.°	62%	1.07
III-1.85-03b	33%	0.016	45.°	30%	0.91
III-1.85-03b	40%	0.025	45.°	37%	0.92
III-1.85-03b	49%	0.030	45.°	41%	0.84
III-1.85-03b	57%	0.033	45.°	44%	0.77
III-1.85-03b	65%	0.040	26.°	96%	1.49
III-1.85-03b	73%	0.040	26.°	96%	1.32
III-1.85-03b	81%	0.045	26.°	99%	1.23
III-1.85-03b	89%	0.050	26.°	100%	1.12
III-1.85-02b	16%	0.017	26.°	78%	4.80
III-1.85-02b	25%	0.023	26.°	79%	3.11
III-1.85-02b	33%	0.028	26.°	80%	2.39
III-1.85-02b	41%	0.033	26.°	82%	2.00

Table B-2 (cont.): Results from beams tested by Birrcher et al. (2009

Member Name	V_a/V_u (exp)	w_k (in.)	θ_{cr} (deg)	V_a/V_u (est)	est/ exp
III-1.85-02b	49%	0.038	26.°	83%	1.71
III-1.85-02b	57%	0.040	26.°	85%	1.49
III-1.85-02b	65%	0.043	26.°	86%	1.32
III-1.85-02b	73%	0.050	26.°	89%	1.22
III-1.85-02b	80%	0.058	26.°	92%	1.14
III-1.2-02	20%	0.012	39.8°	43%	2.14
III-1.2-02	28%	0.020	39.8°	42%	1.50
III-1.2-02	36%	0.028	39.8°	43%	1.19
III-1.2-02	45%	0.033	39.8°	44%	0.99
III-1.2-02	52%	0.035	39.8°	45%	0.86
III-1.2-02	60%	0.040	39.8°	46%	0.77
III-1.2-02	70%	0.045	39.8°	47%	0.67
III-1.2-02	80%	0.045	39.8°	47%	0.59
III-1.2-02	90%	0.050	39.8°	48%	0.54
III-1.2-03	41%	0.016	39.8°	41%	0.99
III-1.2-03	51%	0.020	39.8°	42%	0.83
III-1.2-03	61%	0.030	39.8°	45%	0.74
III-1.2-03	71%	0.040	39.8°	49%	0.69
III-1.2-03	81%	0.046	39.8°	52%	0.64
III-1.2-03	92%	0.058	39.8°	57%	0.62
III-2.5-02	38%	0.010	21.8°	70%	1.86
III-2.5-02	50%	0.025	21.8°	80%	1.59
III-2.5-02	63%	0.035	21.8°	82%	1.31
III-2.5-02	74%	0.050	21.8°	72%	0.97

Table B-2 (cont.): Results from beams tested by Birrcher et al. (2009

Member Name	V_a/V_u (exp)	w_k (in.)	θ_{cr} (deg)	V_a/V_u (est)	est/ exp
III-2.5-03	20%	0.023	21.8°	70%	3.51
III-2.5-03	27%	0.028	21.8°	72%	2.68
III-2.5-03	33%	0.033	21.8°	75%	2.25
III-2.5-03	40%	0.035	21.8°	77%	1.91
III-2.5-03	47%	0.038	21.8°	78%	1.67
III-2.5-03	53%	0.040	21.8°	80%	1.49
III-2.5-03	60%	0.043	21.8°	81%	1.36
III-2.5-03	67%	0.045	21.8°	83%	1.24
III-2.5-03	73%	0.050	21.8°	86%	1.17
III-2.5-03	80%	0.055	21.8°	88%	1.10
IV-2175-1.85-02	27%	0.015	28.4°	72%	2.66
IV-2175-1.85-02	37%	0.025	28.4°	72%	1.95
IV-2175-1.85-02	51%	0.033	28.4°	74%	1.44
IV-2175-1.85-02	62%	0.053	28.4°	80%	1.29
IV-2175-1.85-02	71%	0.060	28.4°	83%	1.16
IV-2175-1.85-02	82%	0.065	28.4°	85%	1.03
IV-2175-1.85-03	33%	0.015	28.4°	63%	1.92
IV-2175-1.85-03	45%	0.023	28.4°	65%	1.45
IV-2175-1.85-03	55%	0.033	28.4°	70%	1.27
IV-2175-1.85-03	64%	0.035	28.4°	71%	1.11
IV-2175-1.85-03	73%	0.043	28.4°	75%	1.03
IV-2175-1.85-03	85%	0.055	28.4°	82%	0.97
IV-2175-2.5-02	39%	0.015	21.8°	69%	1.77
IV-2175-2.5-02	49%	0.020	21.8°	68%	1.38

Table B-2 (cont.): Results from beams tested by Birrcher et al. (2009

Member Name	V_a/V_u (exp)	w_k (in.)	θ_{cr} (deg)	V_a/V_u (est)	est/ exp
IV-2175-2.5-02	59%	0.030	21.8°	78%	1.32
IV-2175-2.5-02	69%	0.035	21.8°	78%	1.13
IV-2175-2.5-02	78%	0.040	21.8°	79%	1.02
IV-2175-2.5-02	87%	0.053	21.8°	83%	0.95
IV-2175-1.2-02	26%	0.023	39.8°	40%	1.52
IV-2175-1.2-02	34%	0.025	39.8°	40%	1.16
IV-2175-1.2-02	43%	0.033	39.8°	40%	0.93
IV-2175-1.2-02	51%	0.040	39.8°	41%	0.80
IV-2175-1.2-02	61%	0.055	39.8°	43%	0.71
IV-2175-1.2-02	68%	0.071	39.8°	50%	0.74
IV-2175-1.2-02	76%	0.090	39.8°	60%	0.78
IV-2175-1.2-02	85%	0.098	39.8°	63%	0.74
IV-2123-1.85-03	29%	0.012	28.4°	100%	3.43
IV-2123-1.85-02	29%	0.018	28.4°	100%	3.45
IV-2123-1.85-02	38%	0.023	28.4°	96%	2.52
IV-2123-1.85-02	48%	0.024	28.4°	96%	2.00
IV-2123-2.5-02	47%	0.020	21.8°	83%	1.78
IV-2123-2.5-02	64%	0.033	21.8°	89%	1.39
IV-2123-2.5-02	98%	0.095	21.8°	65%	0.66
M-03-4-CCC2436	34%	0.013	28.4°	76%	2.21
M-03-4-CCC2436	38%	0.016	28.4°	77%	2.01
M-03-4-CCC2436	41%	0.020	28.4°	78%	1.88
M-03-4-CCC2436	48%	0.025	28.4°	80%	1.68
M-03-4-CCC2436	51%	0.030	28.4°	83%	1.61

Table B-2 (cont.): Results from beams tested by Birrcher et al. (2009

Member Name	V_a/V_u (exp)	w_k (in.)	θ_{cr} (deg)	V_a/V_u (est)	est/ exp
M-03-4-CCC2436	58%	0.030	28.4°	83%	1.43
M-03-4-CCC2436	64%	0.040	28.4°	88%	1.37
M-03-4-CCC2436	71%	0.040	28.4°	88%	1.25
M-03-4-CCC2436	77%	0.050	28.4°	94%	1.22
M-03-4-CCC2436	83%	0.060	28.4°	99%	1.18
M-03-4-CCC2436	92%	0.060	28.4°	99%	1.07
M-03-4-CCC0812	26%	0.020	28.4°	75%	2.88
M-03-4-CCC0812	35%	0.025	28.4°	78%	2.23
M-03-4-CCC0812	43%	0.025	28.4°	78%	1.82
M-03-4-CCC0812	48%	0.030	28.4°	81%	1.71
M-03-4-CCC0812	60%	0.035	28.4°	84%	1.41
M-03-4-CCC0812	67%	0.040	28.4°	88%	1.30
M-03-4-CCC0812	71%	0.040	28.4°	88%	1.23
M-03-4-CCC0812	79%	0.050	28.4°	94%	1.19
M-03-4-CCC0812	87%	0.060	28.4°	99%	1.14
M-03-4-CCC0812	95%	0.060	28.4°	99%	1.05
M-02-4-CCC2436	27%	0.013	28.4°	86%	3.21
M-02-4-CCC2436	32%	0.020	28.4°	86%	2.66
M-02-4-CCC2436	39%	0.025	28.4°	87%	2.25
M-02-4-CCC2436	45%	0.030	28.4°	89%	2.00
M-02-4-CCC2436	51%	0.035	28.4°	91%	1.79
M-02-4-CCC2436	57%	0.045	28.4°	95%	1.66
M-02-4-CCC2436	64%	0.055	28.4°	99%	1.54
M-02-4-CCC2436	71%	0.060	28.4°	100%	1.42

Table B-2 (cont.): Results from beams tested by Birrcher et al. (2009

Member Name	V_a/V_u (exp)	w_k (in.)	θ_{cr} (deg)	V_a/V_u (est)	est/ exp
M-02-4-CCC2436	76%	0.070	28.4°	98%	1.29
				μ	**1.45**
				COV	**51 %**

Table B-3: Results from beams tested by Larson et al. (2013)

Member Name	V_a/V_u (exp)	w_k (in.)	θ_{cr} (deg)	V_a/V_u (est)	est/ exp
DC3-42-1.85-03	33%	0.012	43.°	30%	0.92
DC3-42-1.85-03	39%	0.016	38.°	41%	1.05
DC3-42-1.85-03	52%	0.023	38.°	43%	0.83
DC3-42-1.85-03	65%	0.034	37.°	51%	0.78
DC3-42-1.85-03	78%	0.063	37.°	66%	0.84
DS3-42-1.85-03	46%	0.019	46.°	37%	0.82
DS3-42-1.85-03	57%	0.031	46.°	50%	0.88
DS3-42-1.85-03	69%	0.043	46.°	63%	0.91
DS3-42-1.85-03	80%	0.050	46.°	71%	0.89
DS3-42-1.85-03	88%	0.068	46.°	91%	1.03
DS3-42-1.85-03	92%	0.080	46.°	100%	1.09
SC3-42-1.85-03	36%	0.015	35.°	47%	1.29
SC3-42-1.85-03	48%	0.023	35.°	49%	1.02
SC3-42-1.85-03	60%	0.031	35.°	52%	0.87
SC3-42-1.85-03	72%	0.046	35.°	59%	0.82
SS3-42-1.85-03	43%	0.015	37.°	41%	0.94
SS3-42-1.85-03	54%	0.020	37.°	42%	0.77
SS3-42-1.85-03	65%	0.028	37.°	44%	0.68
SS3-42-1.85-03	76%	0.038	33.°	62%	0.82
SL3-42-1.85-03	40%	0.019	37.°	43%	1.10
SL3-42-1.85-03	49%	0.028	37.°	46%	0.94
SL3-42-1.85-03	59%	0.038	37.°	51%	0.85
SL3-42-1.85-03	69%	0.045	37.°	54%	0.78
SL3-42-1.85-03	79%	0.053	37.°	58%	0.73

Table B-3 (cont.): Results from beams tested by Larson et al. (2013

Member Name	V_a/V_u (exp)	w_k (in.)	θ_{cr} (deg)	V_a/V_u (est)	est/ exp
SL3-42-1.85-03	89%	0.071	37.°	67%	0.76
SS1-75-1.85-03	35%	0.015	32.°	57%	1.62
SS1-75-1.85-03	42%	0.017	32.°	58%	1.38
SS1-75-1.85-03	49%	0.018	32.°	58%	1.19
SS1-75-1.85-03	56%	0.023	32.°	61%	1.08
SS1-75-1.85-03	63%	0.026	32.°	63%	1.00
SS1-75-1.85-03	70%	0.035	32.°	69%	0.98
SS1-75-1.85-03	77%	0.043	32.°	74%	0.96
SS1-75-1.85-03	84%	0.055	32.°	83%	0.98
SS1-75-1.85-03	91%	0.060	32.°	86%	0.95
SS1-42-1.85-03	39%	0.019	31.°	63%	1.62
SS1-42-1.85-03	52%	0.024	31.°	65%	1.25
SS1-42-1.85-03	65%	0.031	31.°	69%	1.06
SS1-42-1.85-03	78%	0.035	31.°	71%	0.91
SS1-42-1.85-03	91%	0.063	31.°	89%	0.98
DS1-42-1.85-03	27%	0.013	28.4°	68%	2.56
DS1-42-1.85-03	31%	0.015	28.4°	68%	2.19
DS1-42-1.85-03	37%	0.017	28.4°	69%	1.88
DS1-42-1.85-03	42%	0.021	28.4°	71%	1.69
DS1-42-1.85-03	52%	0.030	28.4°	76%	1.45
DS1-42-1.85-03	63%	0.035	28.4°	79%	1.25
DS1-42-1.85-03	73%	0.039	28.4°	81%	1.12
DS1-42-1.85-03	78%	0.043	28.4°	84%	1.07
DS1-42-1.85-03	84%	0.048	28.4°	87%	1.04

Table B-3 (cont.): Results from beams tested by Larson et al. (2013

Member Name	V_a/V_u (exp)	w_k (in.)	θ_{cr} (deg)	V_a/V_u (est)	est/ exp
DS1-42-2.50-03	32%	0.014	21.8°	71%	2.24
DS1-42-2.50-03	40%	0.016	21.8°	72%	1.79
DS1-42-2.50-03	56%	0.024	21.8°	75%	1.33
DS1-42-2.50-03	71%	0.035	21.8°	81%	1.14
DS1-42-2.50-03	87%	0.062	21.8°	84%	0.97
DS1-42-2.50-03	95%	0.094	21.8°	80%	0.84
DS1-42-1.85-06	49%	0.013	28.4°	67%	1.36
DS1-42-1.85-06	61%	0.016	28.4°	71%	1.16
DS1-42-1.85-06	74%	0.020	28.4°	77%	1.04
DS1-42-1.85-06	86%	0.028	28.4°	88%	1.02
DS1-42-2.50-06	39%	0.010	21.8°	60%	1.53
DS1-42-2.50-06	53%	0.013	21.8°	64%	1.21
DS1-42-2.50-06	66%	0.015	21.8°	67%	1.02
DS1-42-2.50-06	72%	0.019	21.8°	72%	1.00
DS1-42-2.50-06	80%	0.025	21.8°	81%	1.02
DS1-42-2.50-06	92%	0.033	21.8°	93%	1.01
DL1-42-1.85-06	46%	0.012	28.4°	67%	1.45
DL1-42-1.85-06	57%	0.014	28.4°	70%	1.23
DL1-42-1.85-06	67%	0.017	28.4°	73%	1.10
DL1-42-1.85-06	77%	0.022	28.4°	81%	1.05
DL1-42-1.85-06	87%	0.034	28.4°	97%	1.11
DL1-42-2.50-06	42%	0.012	21.8°	63%	1.48
DL1-42-2.50-06	53%	0.015	21.8°	67%	1.26
DL1-42-2.50-06	64%	0.018	21.8°	71%	1.11

Table B-3 (cont.): Results from beams tested by Larson et al. (2013

Member Name	V_a/V_u (exp)	w_k (in.)	θ_{cr} (deg)	V_a/V_u (est)	est/ exp
DL1-42-2.50-06	75%	0.023	21.8°	79%	1.06
DL1-42-2.50-06	80%	0.026	21.8°	84%	1.06
SS3-42-2.50-03	43%	0.017	21.8°	71%	1.63
SS3-42-2.50-03	54%	0.020	21.8°	72%	1.33
SS3-42-2.50-03	65%	0.026	21.8°	75%	1.15
SS3-42-2.50-03	76%	0.041	21.8°	84%	1.10
SC3-42-2.50-03	43%	0.013	21.8°	71%	1.67
SC3-42-2.50-03	57%	0.023	21.8°	74%	1.31
SC3-42-2.50-03	71%	0.029	21.8°	77%	1.09
DS3-42-2.50-03	33%	0.014	21.8°	71%	2.16
DS3-42-2.50-03	44%	0.021	21.8°	73%	1.67
DS3-42-2.50-03	55%	0.026	21.8°	76%	1.38
DS3-42-2.50-03	66%	0.035	21.8°	81%	1.23
DS3-42-2.50-03	88%	0.073	21.8°	83%	0.95
DL1-42-1.85-03	43%	0.010	28.4°	67%	1.57
DL1-42-1.85-03	55%	0.014	28.4°	67%	1.23
DL1-42-1.85-03	67%	0.019	28.4°	69%	1.04
DL1-42-1.85-03	79%	0.030	28.4°	75%	0.95
DL1-42-1.85-03	91%	0.050	28.4°	89%	0.97
DL1-42-2.50-03	52%	0.015	21.8°	70%	1.34
DL1-42-2.50-03	65%	0.019	21.8°	71%	1.10
DL1-42-2.50-03	78%	0.029	21.8°	76%	0.98
SL3-42-1.85-06	45%	0.010	28.4°	59%	1.32
SL3-42-1.85-06	52%	0.015	28.4°	65%	1.25

Table B-3 (cont.): Results from beams tested by Larson et al. (2013

Member Name	V_a/V_u (exp)	w_k (in.)	θ_{cr} (deg)	V_a/V_u (est)	est/ exp
SL3-42-1.85-06	60%	0.018	28.4°	69%	1.15
SL3-42-1.85-06	67%	0.025	28.4°	79%	1.17
SL3-42-1.85-06	75%	0.025	28.4°	79%	1.05
SL3-42-1.85-06	82%	0.030	28.4°	85%	1.04
SL3-42-1.85-06	90%	0.038	28.4°	94%	1.05
DC1-42-1.85-06	44%	0.012	28.4°	89%	2.03
DC1-42-1.85-06	59%	0.018	28.4°	97%	1.66
SS1-42-2.50-03	33%	0.011	21.8°	73%	2.19
SS1-42-2.50-03	42%	0.018	21.8°	71%	1.70
SS1-42-2.50-03	58%	0.031	21.8°	78%	1.33
SS1-42-2.50-03	75%	0.045	21.8°	86%	1.15
SS1-42-2.50-03	92%	0.090	21.8°	81%	0.88
SL1-42-2.50-03	33%	0.012	21.8°	68%	2.04
SL1-42-2.50-03	40%	0.018	21.8°	70%	1.75
SL1-42-2.50-03	53%	0.025	21.8°	74%	1.38
SL1-42-2.50-03	67%	0.031	21.8°	78%	1.17
SL1-42-2.50-03	80%	0.048	21.8°	89%	1.12
SL1-42-2.50-03	93%	0.095	21.8°	81%	0.87
DS1-42-1.85-06/03	20%	0.012	28.4°	68%	3.31
DS1-42-1.85-06/03	31%	0.014	28.4°	71%	2.32
DS1-42-1.85-06/03	41%	0.019	28.4°	79%	1.92
DS1-42-1.85-06/03	51%	0.025	28.4°	87%	1.70
DS1-42-1.85-06/03	61%	0.029	28.4°	92%	1.50
DS1-42-1.85-06/03	72%	0.035	28.4°	99%	1.38

Table B-3 (cont.): Results from beams tested by Larson et al. (2013

Member Name	V_a/V_u (exp)	w_k (in.)	θ_{cr} (deg)	V_a/V_u (est)	est/ exp
DS1-42-1.85-06/03	82%	0.038	28.4°	100%	1.22
DS1-42-2.50-06/03	24%	0.013	21.8°	67%	2.76
DS1-42-2.50-06/03	36%	0.018	21.8°	74%	2.04
DS1-42-2.50-06/03	49%	0.024	21.8°	84%	1.72
DS1-42-2.50-06/03	61%	0.026	21.8°	88%	1.44
DS1-42-2.50-06/03	73%	0.034	21.8°	98%	1.35
DC1-42-1.85-03	30%	0.013	28.4°	80%	2.69
DC1-42-1.85-03	44%	0.019	28.4°	82%	1.84
DC1-42-1.85-03	59%	0.024	28.4°	85%	1.43
DC1-42-1.85-03	74%	0.039	28.4°	94%	1.28
				μ	**1.29**
				COV	**29 %**

References

American Association of State Highway and Transportation Officials (AASHTO). (2010) *AASHTO bridge element inspection guide manual* (1st ed.).

American Association of State Highway and Transportation Officials (AASHTO). (2005). *Guide manual for condition evaluation and LRFR of highway bridges* (2005 interim revisions).

Acevedo, A. B., Bentz, E. C., & Collins, M. P. (2008). *Influence of clamping stresses on the shear strength of concrete slabs under uniform loads*. ROSE School, IUSS Press.

American Society of Civil Engineers (ASCE). (2017). *2017 Infrastructure Report Card*.

Abi Shdid, C., Ansley, M., & Hamilton III, H. (2006). Visual rating and strength testing of 40-year-old precast prestressed concrete bridge piling. *Transportation Research Record: Journal of the Transportation Research Board*, (1975), 3-9.

Aguilar, G. (2011). *Effect of high-strength concrete on web reinforcement requirements for reinforced concrete bridge girders* (Doctoral dissertation). Purdue University, West Lafayette, Indiana.

Alembagheri, M., & Ghaemian, M. (2013). Damage assessment of a concrete arch dam through nonlinear incremental dynamic analysis. *Soil Dynamics and Earthquake Engineering*, *44*, 127–137.

Bentz, E. C., Vecchio, F. J., & Collins, M. P. (2006). Simplified modified compression field theory for calculating shear strength of reinforced concrete elements. *ACI Structural Journal*, *103*(4), 614–624.

Birrcher, D., Tuchscherer, R., Huizinga, M., Bayrak, O., Wood, S. L., & Jirsa, J. O. (2009). *Strength and serviceability design of reinforced concrete deep beams* (No. FHWA/TX-09/0-5253-1).

Bracci, J. M., Keating, P. B., & Hueste, M. B. D. (2000). *Cracking in RC bent caps* (No. FHWA/TX-01/1851-1,).

Calvi, P. M. (2015). *A theory for the shear behaviour of cracks providing a basis for the assessment of cracked reinforced concrete structures* (Doctoral dissertation). University of Toronto, Toronto, Ontario.

Comite Euro-International du Beton (CEB-FIP). (1978). *Model Code for Concrete Structures* (3rd ed.), 348 pp.

Comite Euro-International du Beton (CEB-FIP). (1990). *Model Code for Concrete Structures*, 437 pp.

Chowdhury, S. H. and Loo, Y. C. (2001). A new formula for prediction of crack widths in reinforced and partially prestressed concrete beams. *Advances in Structural Engineering, 4*(2), 101-110.

De Silva, S., Mutsuyoshi, H., & Witchukreangkrai, E. (2008). Evaluation of shear crack width in i-shaped prestressed reinforced concrete beams. *Journal of Advanced Concrete Technology, 6*(3), 443-458.

Deluce, J. R. (2011). *Cracking Behaviour of Steel Fiber Reinforced Concrete Containing Conventional Steel Reinforcement* (Master's thesis). University of Toronto, Toronto, Ontario.

Deluce, J. R., Lee, S., and Vecchio, F. J. (2014). Crack model for steel fiber-reinforced concrete members containing conventional reinforcement. *ACI Structural Journal, 111*(1), 93-102.

Ebrahimkhanlou, A., Farhidzadeh, A., & Salamone, S. (2016). Multifractal analysis of crack patterns in reinforced concrete shear walls. *Structural Health Monitoring*, *15*(1), 81–92.

European Committee for Standardization. (1991). *Eurocode 2: Design of concrete structures – Part 1: General rules and rules for buildings*.

European Committee for Standardization. (2004). *Eurocode 2: Design of concrete structures – Part 1-1: General rules and rules for buildings*.

Farhidzadeh, A., Dehghan-Niri, E., Moustafa, A., Salamone, S., & Whittaker, A. (2013). Damage assessment of reinforced concrete structures using fractal analysis of residual crack patterns. *Experimental Mechanics*, *53*(9), 1607–1619.

FHWA. (2012). Bridge inspector's reference manual: Volume 1 (Report No. FHWA NHI 12-049).

FHWA. (2012). Bridge inspector's reference manual: Volume 2 (Report No. FHWA NHI 12-050).

FHWA. (1995). Recording and coding guide for the structure inventory and appraisal of the nation's bridges (Report No. FHWA-PD-96-001).

fib (International Federation for Structural Concrete). (2013). *Model code 2010: Final draft*. Volume 1, International Federation for Structural Concrete, Bulletin No. 65, Lausanne, Switzerland, March 2012, 350 pp.

Gulkan, P., & Yakut, A. (1996). An expert system for reinforced concrete structural damage quantification. *Special Publication*, *162*, 53–72.

Higgins, C., Miller, T., H., Rosowsky, D., V., Yim, S., C., Potisuk, T., Daniels, T., K., Nicholas, B., S., Robelo, M., J., Lee, A., Y. and Forrest, R., W. (2004). *Assessment methodology for diagonally cracked reinforced concrete deck girders* (No. FHWA-OR-RD-05-04,).

Hillerborg, A., Modéer, M., & Petersson, P. E. (1976). Analysis of crack formation and crack growth in concrete by means of fracture mechanics and finite elements. *Cement and Concrete Research*, *6*(6), 773–782.

International Atomic Energy Association (IAEA). (2002). *Guidebook on non-destructive testing of concrete structures*. Vienna, Austria.

Kabir, S., Rivard, P., He, D.-C., & Thivierge, P. (2009). Damage assessment for concrete structure using image processing techniques on acoustic borehole imagery. *Construction and Building Materials*, *23*(10), 3166 – 3174.

Kono, S., Bechtoula, H., Sakashita, M., Tanaka, H., Watanabe, F., & Eberhard, M. O. (2006). Damage Assessment of Reinforced Concrete Columns Under High Axial Loading. *Special Publication*, *237*, 165–176.

Lantsoght, E. O., van der Veen, C., Walraven, J. C., & Boer, A. D. (2016). Case study on aggregate interlock capacity for the shear assessment of cracked reinforced-concrete bridge cross sections. *Journal of Bridge Engineering*, *21*(5), 04016004.

Larson, N., Gomez, E. F., Garber, D., Bayrak, O., & Ghannoum, W. (2013). *Strength and serviceability design of reinforced concrete inverted-T beams* (No. FHWA/TX-13/0-6416-1).

Li, B., Nair, A., & Kai, Q. (2012). Residual axial capacity of reinforced concrete columns with simulated blast damage. *Journal of Performance of Constructed Facilities*, *26*(3), 287–299.

Lee, J., Lee, D. H., Lee, J., & Choi, S. (2015). Shear behavior and diagonal crack width for RC beams with high strength shear reinforcement. *ACI Structural Journal, 112*(3)*, 323-334.*

Lopes, R., & Betrouni, N. (2009). Fractal and multifractal analysis: A review. *Medical Image Analysis*, *13*(4), 634–649.

Melchor-Lucero, O., & Ferregut, C. (1996). Earthquake damage assessment of reinforced concrete members using an expert system. In *Eleventh World Conference on Earthquake Engineering*, *Acapulco, Mexico*.

Michigan Department of Transportation (MDOT). (2011). *MDOT BSIR rating guides*.

Montana Department of Transportation (MDT). (2015). *Bridge inspection and rating manual*.

Ohio Department of Transportation (ODOT). (2014). *Manual of bridge inspection*.

Oregon Department of Transportation (ODOT). (2009). *2009 bridge inspection pocket coding guide*.

Paal, S. G., Jeon, J.-S., Brilakis, I., & DesRoches, R. (2015). Automated damage index estimation of reinforced concrete columns for post-earthquake evaluations. *Journal of Structural Engineering*, *141*(9), 04014228.

Pang, X. (1991). Constitutive laws of reinforced concrete in shear (Doctoral dissertation). University of Houston, Houston, Texas.

Park, S., Stubbs, N., Bolton, R., Choi, S., & Sikorsky, C. (2001). Field verification of the damage index method in a concrete box-girder bridge via visual inspection. *Computer-Aided Civil and Infrastructure Engineering*, *16*(1), 58–70.

Pennsylvania Department of Transportation (PennDOT). (2009). *PENNDOT publication #100A*.

Proestos, G., T., Bae, G., M., Lee, S., C., Bentz, E., C., Collins, M., P. and Cho, J., Y. (2015). Influence of High-Strength Reinforcing Bars on Shear Response of Reinforced Concrete Nuclear Power Plant Wall Elements, *ACI Structural Journal*, under review.

Ruggiero, D., M., Bentz E., C. and Collins, M., P. (2014). Behaviour of reinforced concrete panels subjected to reversed-cyclic shear loads, Proc. of the 10th fib International PhD Symposium in Civil Engineering July 21 to 23, 2014, Université Laval, Québec, Canada.

Sain, T., & Kishen, J. M. C. (2007). Prediction of fatigue strength in plain and reinforced concrete beams. *ACI Structural Journal*, *104*(5), 621–628.

Schlaich, J., Schafer, K., & Jennewein, M. (1987). Towards a consistent design of reinforced concrete structures. *PCI Journal*, 32(3), 74-150.

Sherwood, E. G. (2008). One-way shear behaviour of large, lightly-reinforced concrete beams and slabs. (Doctoral dissertation). University of Toronto, Toronto, Ontario.

Susetyo, J. (2009). Fibre reinforcement for shrinkage crack control in prestressed, precast segmental bridges (Doctoral dissertation). University of Toronto, Toronto, Ontario.

Talley, K. G., Arrellaga, J., & Breen, J. E. (2014). Computational modeling of existing damage in concrete bridge columns. *Journal of Structural Engineering, ASCE*, *140*(12), 06014006.

Texas Department of Transportation (TxDOT). (2013). *Bridge inspection manual*.

Uzel, A. (2003). Shear design of large footings (Doctoral dissertation). University of Toronto, Toronto, Ontario.

Vecchio, F. J. (1989). Nonlinear finite element analysis of reinforced concrete membranes. *ACI Structural Journal*, *86*(1), 26-35.

Vecchio, F. J. (2000). Disturbed stress field model for reinforced concrete: Formulation. *Journal of Structural Engineering, 126*(9), 1070–1077.

Vecchio, F. J. (2001). Non-linear finite element analysis of reinforced concrete: at the crossroads? *Structural Concrete*, *2*(4), 201–212.

Vecchio, F. J., & Collins, M. P. (1986, March). The modified compression-field theory for reinforced concrete elements subjected to shear. In *Journal Proceedings* (Vol. 83, No. 2, pp. 219-231).

Veletzos, M. J., Panagiutou, M., Restrepo, J. I., & Sahs, S. (2008). *Visual Inspection & Capacity Assessment of Earthquake Damaged Reinforced Concrete Bridge Elements* (No. SSRP-06/19).

Walraven, J. C. (1980). Aggregate interlock : a theoretical and experimental analysis. Delft Univ. Pr., Delft.

Walraven, J. C. (1981a). Aggregate interlock. *Cement*, *33*(6), 406 – 412.

Walraven, J. C. (1981b). Fundamental Analysis of Aggregate Interlock. *Journal of the Structural Division*, *107*(11), 2245–2270.

Wang, J., Shi, Z., & Nakano, M. (2013). Strength degradation analysis of an aging RC girder bridge using FE crack analysis and simple capacity-evaluation equations. *Engineering Fracture Mechanics*, *108*, 209–221.

Wong, P.S., Vecchio, F. J., & Trommels, H. (2013). *VecTor2 & FormWorks user's manual* (2nd ed.). University of Toronto, Toronto, Ontario, 318 pp.

Xiang, Y., Xu, J., & Wu, Q. (2012). Crack width calculation methods of reinforced concrete bridges and application of box girder bridge. *Journal of Highway and Transportation Research and Development, 6*(3), 39-43.

Yoon, Y., Cook, W. D., & Mitchell, D. (1996). Minimum shear reinforcement in normal, medium, and high-strength concrete beams. *ACI Structural Journal, 93*(5), 576-584.

Zhu, R. R. H., Wanichakorn, W., Hsu, T. T. C., & Vogel, J. (2003). Crack width prediction using compatibility-aided strut-and-tie model. *ACI Structural Journal*, *100*(4), 413–421.